The Astrophysical Journal, 698:1–27, 2009 June 10 doi:10.1088/0004-637X/698/1/1


# THE LAST GASP OF GAS GIANT PLANET FORMATION: A *SPITZER* STUDY OF THE 5 Myr OLD CLUSTER NGC 2362

Thayne Currie[1], Charles J. Lada[1], Peter Plavchan[2], Thomas P. Robitaille[1], Jonathan Irwin[1,3], and Scott J. Kenyon[1]
[1] Harvard-Smithsonian Center for Astrophysics, 60 Garden Street, Cambridge, MA 02140, USA; tcurrie@cfa.harvard.edu, clada@cfa.harvard.edu, trobitaille@cfa.harvard.edu, jirwin@cfa.harvard.edu, skenyon@cfa.harvard.edu
[2] NASA Exoplanet Science Institute, California Institute of Technology, CA, USA; plavchan@ipac.caltech.edu
[3] Institute of Astronomy, University of Cambridge, Cambridge, UK
*Received 2008 August 27; accepted 2009 March 15; published 2009 May 19*

## ABSTRACT

Expanding upon the Infrared Array Camera (IRAC) survey from Dahm & Hillenbrand, we describe *Spitzer* IRAC and Multiband Imaging Photometer for *Spitzer* observations of the populous, 5 Myr old open cluster NGC 2362. We analyze the mid-IR colors of cluster members and compared their spectral energy distributions (SEDs) to star+circumstellar disk models to constrain the disk morphologies and evolutionary states. Early/intermediate-type confirmed/candidate cluster members either have photospheric mid-IR emission or weak, optically thin IR excess emission at $\lambda \geqslant 24$ $\mu$m consistent with debris disks. Few late-type, solar/subsolar-mass stars have primordial disks. The disk population around late-type stars is dominated by disks with inner holes (canonical "transition disks") and "homologously depleted" disks. Both types of disks represent an intermediate stage between primordial disks and debris disks. Thus, in agreement with previous results, we find that multiple paths for the primordial-to-debris disk transition exist. Because these "evolved primordial disks" greatly outnumber primordial disks, our results undermine standard arguments in favor of a $\lesssim 10^5$ yr timescale for the transition based on data from Taurus–Auriga. Because the typical transition timescale is far longer than $10^5$ yr, these data also appear to rule out standard ultraviolet photoevaporation scenarios as the primary mechanism to explain the transition. Combining our data with other *Spitzer* surveys, we investigate the evolution of debris disks around high/intermediate-mass stars and investigate timescales for giant planet formation. Consistent with Currie et al., the luminosity of 24 $\mu$m emission in debris disks due to planet formation peaks at ≈10–20 Myr. If the gas and dust in disks evolve on similar timescales, the formation timescale for gas giant planets surrounding early-type, high/intermediate-mass ($\gtrsim 1.4\ M_\odot$) stars is likely 1–5 Myr. Most solar/subsolar-mass stars detected by *Spitzer* have SEDs that indicate their disks may be actively leaving the primordial disk phase. Thus, gas giant planet formation may also occur by ∼5 Myr around solar/subsolar-mass stars as well.

*Key words:* circumstellar matter – open clusters and associations (individual: NGC 2362) – planetary systems: formation – planetary systems: protoplanetary disks – stars: pre-main sequence

*Online-only material:* machine-readable tables

## 1. INTRODUCTION

Primordial circumstellar disks of gas and small dust grains surround the vast majority of ≈1 Myr old stars and are the building blocks of planets (Lada & Adams 1992; Kenyon & Hartmann 1995). Observable as emission in excess of the stellar photosphere at infrared IR wavelengths, primordial disks accrete gas onto the host star and have strong, optically thick emission comparable in luminosity to the stellar photosphere ($L_d/L_\star \sim$ 0.1–1). Small dust grains in primordial disks comprise the seed material for the cores of planets; the gaseous envelopes of gas giant and ice giant planets form from the circumstellar gas in these disks.

Primordial disks disappear on ∼3–10 Myr timescales. In clusters with ages of ∼3 Myr, many disks have much less emission than typical primordial disks at wavelengths $\lesssim 10$ $\mu$m (e.g., Lada et al. 2006; Hernandez et al. 2007a). Primordial disks disappear around nearly all stars by ∼10–15 Myr (e.g., Currie et al. 2007c). Disks surrounding ⩾10 Myr old stars are typically optically thin *debris disks* with weaker IR emission (Rieke et al. 2005; Chen et al. 2005; Currie et al. 2007c, 2008a, 2008b; Forbrich et al. 2008; Hillenbrand et al. 2008; Plavchan et al. 2009) and little evidence for substantial reservoirs of circumstellar gas (e.g., Dahm 2005b; Currie et al. 2007a). Because dust from debris disks can be removed by stellar radiation on very short ($\lesssim$0.1 Myr) timescales (e.g., Burns et al. 1979; Takeuchi & Artymowicz 2001; Plavchan et al. 2005), the dust requires an active replenishment source from collisions between larger objects. Thus, debris disks are signposts for active planet formation (e.g., Backman & Paresce 1993; Kenyon & Bromley 2004, 2008).

While debris disks may trace active terrestrial and icy planet formation, they do not trace the final stages of active gas giant planet formation, where massive cores accrete large gaseous envelopes. Debris disk have very low masses of residual gas, $\ll 1\ M_\oplus$ (e.g., Zuckerman et al. 1995; Chen & Kamp 2004; Roberge & Weinberger 2008; France et al. 2007). This mass is too small to contribute to a gaseous envelope with a mass comparable to those found in Jupiter and Saturn.

The timescale for the disappearance of primordial disks and the subsequent dominance of debris disks has important implications for gas giant planet formation. In the core accretion theory for gas giant planet formation (e.g., Pollack et al. 1996), $\gtrsim$Mars-mass protoplanetary cores can accrete a gaseous envelope, which is in hydrostatic equilibrium. However, once the cores reach ≈5–10 $M_\oplus$ in mass, they can rapidly accrete a much more massive envelope. If the nebular gas disperses before the critical core mass is reached, gas giants fail to

form. Typical timescales for massive cores to form range from ≈1 Myr (Rafikov 2004; Currie 2005; Kenyon & Bromley 2009) to 10 Myr (Pollack et al. 1996; Rice & Armitage 2003). Because debris disks are gas poor, the time when most primordial disks evolve into debris disks sets an empirical upper limit for the formation timescale of gas giant planets.

Identifying *how* primordial disks evolve into debris disks may also have important implications for planet formation. Early work from *Infrared Astronomical Satellite* and ground-based data (specifically Taurus–Auriga) suggested that ∼1%–10% of ≈1 Myr old stars have so-called "transition disks": disks with levels of mid-IR emission in between those of stars surrounded by primordial disks and stars lacking a disk as determined from color–color diagrams (e.g., Hartigan et al. 1990; Skrutskie et al. 1990; Simon & Prato 1995; Wolk & Walter 1996). Later studies of "transition" disks began to associate the term with a specific disk morphology: disks with inner regions that are optically thin and thus depleted or devoid of gas and dust but colder, outer regions with optically thick emission (e.g., Calvet et al. 2005). If all disks follow make this transition, then disks are cleared from the inside out with a transition time of $\sim 10^4$–$10^5$ yr. Plausible physical processes for removing primordial disks must then reproduce this rapid transition timescale. Ultraviolet photoevaporation models are successful in clearing disks within ∼0.01–0.1 Myr (Clarke et al. 2001; Alexander et al. 2006).

However, recent spectral energy distribution (SED) analysis of some 2–3 Myr old stars indicates that they may follow a different evolutionary sequence from primordial disks to debris disks (Lada et al. 2006; Currie & Kenyon 2009). Their near-to-mid-IR fluxes are consistent with a "homologous depletion" in disk emission at all wavelengths through 24 $\mu$m instead of an "inside out" evolution, indicative of a reduced mass of small ($\lesssim$100 $\mu$m–1 mm) dust grains at all stellocentric distances (Wood et al. 2002) that could result from the coagulation of dust into 1 mm–1 km-sized planetesimals and depletion of solid material by accretion onto the star. If many disks evolve from primordial disks to debris disks along this alternate path, then the primordial-to-debris disk transition timescale estimated from the frequency of canonical "transition disks" will be underestimated. Furthermore, if most primordial disks last longer than ∼1 Myr, the frequency of "transition disks" around 1 Myr old stars may be low either because the transition timescale is fast *or* because most disks simply have not had enough time to start leaving the primordial disk phase. If the latter is the correct interpretation, then the transition timescale for many disks could be much longer. Observations of disks at slightly greater, ∼4–5 Myr ages can further test whether there are multiple pathways from primordial disks to debris disks and can better constrain the primordial-to-debris disk transition timescale.

In this paper, we investigate the primordial-to-debris disk transition in the open cluster NGC 2362 in Canis Major ($\alpha_{2000} = 7^h18^m48^s$, $\delta_{2000} = -24°57'00''.0$). With an age of ∼4–5 Myr (Dahm 2005a; Mayne & Naylor 2008), NGC 2362 lies between the epoch when most stars have optically thick primordial disks (∼1 Myr) and the epoch where primordial disks are exceedingly rare (∼10 Myr). While the cluster is very distant (∼1.48 kpc), it is also massive (greater than 500 $M_\odot$). Because of its mass, even nondetections of cluster stars with the Multiband Imaging Photometer for *Spitzer* (MIPS) 24 $\mu$m channel can help constrain the source SEDs and thus the disk evolutionary state (Currie et al. 2007b).

This paper builds upon the study of NGC 2362 by Dahm & Hillenbrand (2007) who focus on Infrared Array Camera (IRAC) observations of 337 candidate/confirmed cluster members and find evidence for disks surrounding many late-type stars. Here we add MIPS 24 $\mu$m data to extend the previous *Spitzer* wavelength coverage of cluster members. We also re-reduce and re-analyze IRAC data and expand the membership sample so that we can include candidate cluster members not studied by Dahm & Hillenbrand (2007). MIPS 24 $\mu$m data probes disk emission that can come from dust colder than the ice sublimation temperature ($T \sim 170$ K). Therefore, our knowledge of the disk population now extends from the warm, inner terrestrial zone regions to cooler, outer regions where gas giant planets may form. The combination of MIPS and IRAC data allow us to better discriminate between disk evolutionary states.

We organize our study as follows. In Section 2, we describe IRAC and MIPS photometry of the NGC 2362 field and ancillary data used to identify *Spitzer* counterparts to known and candidate cluster members. Section 3 focuses on the IRAC+MIPS colors of (candidate) cluster members, providing a first-order constraint on the mid-IR properties of disks in NGC 2362. To constrain the evolutionary state of MIPS-detected cluster members, we compare the observed SEDs to predictions for (evolved) primordial disks and debris disks in Section 4. Section 5 draws inferences about the timescale for gas giant planet formation and the primordial-to-debris disk transition from these data by comparing them with *Spitzer* results for other $\lesssim$10–15 Myr old clusters. We conclude with a brief summary of the paper, discuss our results in the context of other recent work, and discuss future work that can build on our results.

## 2. DATA

### 2.1. Spitzer Observations, Image Processing, and Photometry

#### 2.1.1. IRAC Data

NGC 2362 was observed with the IRAC (Fazio et al. 2004) on 2004 March 3 as a part of the Guaranteed Time Observations (GTO) program (Program ID 37). IRAC data cover an area of ∼0.3 deg$^2$ centered near $\alpha_{2000} \sim 07^h19^m00^s$, $\delta_{2000} \sim -24°27'00''$. IRAC observations were taken in high-dynamic range mode with 0.4 s and 10.4 s exposures. Sources were observed at two dither points yielding an average integration time/pixel of ∼20.8 s for the long exposures.

The IRAC Basic Calibration Data (BCD) require additional post-BCD processing before mosaicing. Specifically, the BCD frames at [3.6] and [4.5] show strong evidence for column pulldown and "striping" effects, which affect pixel flux densities by up to ≈0.5 MJy sr$^{-1}$. The [5.8] and [8] channel BCD frames show evidence for cosmic-ray hits, which are especially numerous in the [5.8] filter. Finally, the automatically produced post-BCD mosaics at [3.6] and [4.5] contain background level mismatch of up to ∼0.1 MJy sr$^{-1}$ near bright stars, which causes a noticeable "tiling" effect.

We cleaned the IRAC data according to the methods described by Currie et al. (2008b), applying the array-dependent correction for point sources (Quijada et al. 2004) and mitigating image artifacts using modified versions of the *muxstriping* and *column pulldown* algorithms available as contributed software on the *Spitzer Science Center* Web site. Final image processing and mosaicing was performed using the MOPEX/APEX pipeline (Makovoz & Marleau 2005). Prior to mosaicing, we applied

the overlap corrector with bright source masking and $3\sigma$ outlier clipping to match the background levels between BCD frames. For cosmic-ray rejection, we used the *r*-masks for each BCD frame supplemented by the *mosaic outlier* and *dual outlier* modules, which removed nearly all cosmic rays. Finally, both the IRAC and MIPS data were mosaiced together using a bicubic interpolation with outlier rejection. The final mosaics were inspected and cleared of image artifacts or pattern noise that could compromise the photometry.

For the IRAC photometry, we perform source finding and aperture photometry using the IDLPHOT package and SExtractor (Bertin & Arnouts 1996). For source identification, we determined the background rms level ($\sigma_{\rm bkgd,rms}$) for each IRAC mosaic using SExtractor. Sources were identified as groups of pixels with fluxes $\geqslant 3\sigma_{\rm bkgd,rms}$ in all filters using the *find.pro* routine. These sources lists were used as input for aperture photometry with the *aper.pro* routine. The source flux was computed in a 2 pixel ($\sim 2\farcs44$) and 3 pixel ($\sim 3\farcs66$) aperture radius with the local background calculated from a 4 pixel thick annulus surrounding each source extending from 2–6 and 3–7 pixels. We multiplied the source fluxes by the appropriate aperture corrections given in the IRAC data handbook, version 3.0.[4] We fine-tuned the aperture correction by first comparing photometry for bright, unsaturated ($\sim$10th–12th magnitude) stars derived above with photometry derived using a 10 pixel aperture and background annulus of 12–20 pixels, which requires no aperture correction. Additionally, we then compared our results with photometry for bright stars measured using a 5 pixel aperture with a 12–20 pixel background annulus.

Photometry from the 2 and 3 pixel apertures show excellent agreement through $\sim$13th (14th) magnitude for the [5.8] and [8] ([3.6] and [4.5]) channels with dispersions of $\ll$0.025 mag. The dispersion increases to $\sim$0.1–0.2 mag beyond these limits. The measured pixel area of $\geqslant$13th magnitude stars is enclosed by the 2 pixel aperture radius. Using the 2 pixel aperture may introduce $\sim$1%–2% uncertainties in the spatial variation of the aperture correction but results in a higher signal to noise, which is important for obtaining accurate photometry of stars whose fluxes are $<10\sigma_{\rm bkgd,rms}$. Furthermore, NGC 2362 is a massive cluster projected against the densely populated galactic plane. Source crowding in the sensitive [3.6] and [4.5] filters can be severe. Several stars in the cluster center appear partially blended with the 3 pixel aperture used. Therefore, we chose photometry from the 2 pixel aperture in all filters for all stars. The final IRAC catalogs were trimmed of sources lying within 5 pixels of the image edges. We combine the IRAC catalogs with the Two Micron All Sky Survey (2MASS) $JHK_s$ catalog using a $2''$ matching radius, resulting in 6916, 7075, 4875, and 3855 matches in the [3.6], [4.5], [5.8], and [8] channels.

The photometric errors are calculated from the Poisson error in the source counts, the read noise, the Poisson error in the background level, and the uncertainty in the background.[5] Figure 1 shows the number counts of IRAC-detected sources with 2MASS counterparts as a function of magnitude. The source counts peak at [3.6] $\sim$ 15.5, [4.5] $\sim$ 15.5, [5.8] $\sim$ 15.0, and [8] $\sim$ 14.25–14.5. IRAC approaches the $10\sigma$ limits at [3.6] $\sim$ 15.75, [4.5] $\sim$ 15.75, [5.8] $\sim$ 13.5, and [8] $\sim$ 13.25. The $5\sigma$ limits for [5.8] and [8] are [5.8] $\sim$ 14.8 and [8] $\sim$ 14.4. Source counts for [3.6] and [4.5] peak before the $10\sigma$ limit is reached because of incompleteness in the 2MASS catalog.

[4] http://ssc.spitzer.caltech.edu/irac/dh/iracdatahandbook3.0.pdf

[5] See https://lists.ipac.caltech.edu/pipermail/irac-ig/2007-February/000037.html

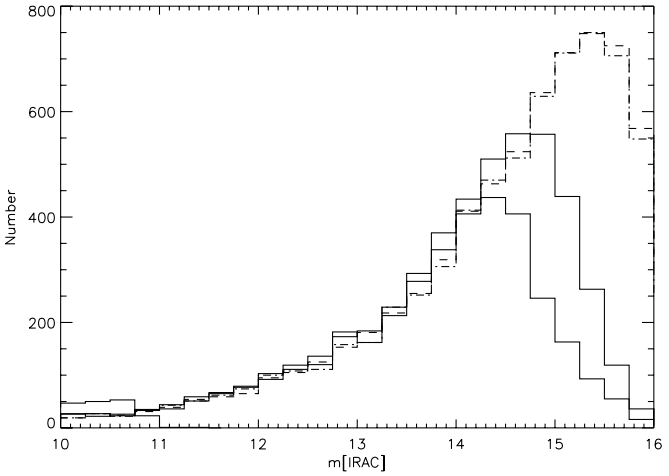


**Figure 1.** Histogram of IRAC detections with 2MASS counterparts. The 5.8 $\mu$m (triple-dot-dashed) and 8 $\mu$m (solid) source counts peak at $m$[IRAC] $\sim$ 15 and 14.25, respectively. The 3.6 $\mu$m (dash-dotted) and 4.5 $\mu$m (dashed line) both peak at $m$[IRAC] $\sim$ 15.5.

### 2.1.2. MIPS 24 $\mu$m Data

NGC 2362 was imaged with the MIPS (Rieke et al. 2004) on 2004 March 17 also as a part of the GTO program (ID 58). MIPS data cover $\sim$0.5 deg$^2$ on the sky with boundaries of $\alpha_{2000} \sim 07^{\rm h}17^{\rm m}45^{\rm s}$ to $07^{\rm h}20^{\rm m}00^{\rm s}$ and $\delta_{2000} \sim -25^\circ26'00''$ to $-24^\circ33'00''$. MIPS 24 $\mu$m observations were taken in scan mode with an integration time per pixel of 80 s. Background cirrus levels at 24 $\mu$m are low ($\approx$19 MJy sr$^{-1}$) and vary by less than $\sim$0.1 MJy sr$^{-1}$ for most of the field. Two regions centered on $\alpha_{2000} \sim 07^{\rm h}18^{\rm m}8^{\rm s}$, $\delta_{2000} \sim -25^\circ16'00''$ and $\alpha_{2000} \sim 07^{\rm h}19^{\rm m}30^{\rm s}$, $\delta_{2000} \sim -24^\circ51'30''$ have slightly higher background levels of $\approx$19.5 MJy sr$^{-1}$. The MIPS BCD data are largely free of artifacts.

Because the MIPS point-spread function is well characterized, we perform photometry on the 24 $\mu$m MIPS data using pixel response function (PRF) fitting with APEX (Makovoz & Khan 2005). We detect 1761 sources at [24] with signal-to-noise ratio (S/N) $>$ 3. Using a $2''$ matching radius, we identify 447 MIPS 24 $\mu$m sources with 2MASS counterparts. Figure 2 shows that the source counts peak at [24] $\sim$ 10.5 ($\sim$460 $\mu$Jy); the ($5\sigma$) $10\sigma$ limits are [24] $\sim$ (10.5) 9.75.[6] Table 1 lists the full photometric catalog of 8642 sources on the IRAC/MIPS fields with 2MASS counterparts and a detection in at least one IRAC and/or MIPS channel. Figure 3 shows a three-color image of NGC 2362 made with the 4.5 $\mu$m and 8 $\mu$m IRAC filters (blue and green) and MIPS 24 $\mu$m filter (red). Most sources discussed in this paper lie within $\sim 7'$ of $\tau$ CMa, near the center of the mosaic and interior to the region with slightly higher 24 $\mu$m background (right-hand side of the figure).

### 2.2. Ancillary Data: Identifying Cluster Members

In the absence of proper motion data, we establish cluster membership by identifying stars with indicators of youth. Most intermediate and late-type young stars are chromospherically active and thus are luminous X-ray sources (e.g., Preibisch & Feigelson 2005). Chromospheric activity as well as circumstellar gas accretion onto a star can result in $H_\alpha$ emission, a common feature in the optical spectra of stars with

[6] The uncertainties quoted here do not include the zero-point uncertainty, which is $\approx$4%.

**Table 1**
Photometry Catalog for All Stars on the NGC 2362 Field

| Number | R.A. | Decl. | $J$ | $H$ | $K_s$ | [3.6] | $\sigma$([3.6]) | [4.5] | $\sigma$([4.5]) | [5.8] | $\sigma$([5.8]) | [8] | $\sigma$([8]) | [24] | $\sigma$([24]) |
|---|---|---|---|---|---|---|---|---|---|---|---|---|---|---|---|
| 1 | 110.0939 | −25.1644 | 13.729 | 13.486 | 13.379 | 13.267 | 0.011 | 0.000 | 0.000 | 13.185 | 0.070 | 0.000 | 0.000 | 99.000 | 0.000 |
| 2 | 110.1280 | −25.3220 | 12.178 | 11.345 | 11.118 | 0.000 | 0.000 | 0.000 | 0.000 | 0.000 | 0.000 | 0.000 | 0.000 | 10.021 | 0.184 |
| 3 | 110.0985 | −25.1656 | 12.275 | 12.206 | 12.014 | 11.964 | 0.005 | 0.000 | 0.000 | 0.000 | 0.000 | 0.000 | 0.000 | 99.000 | 0.000 |
| 4 | 110.0921 | −25.1472 | 16.153 | 15.419 | 15.431 | 15.186 | 0.039 | 0.000 | 0.000 | 0.000 | 0.000 | 0.000 | 0.000 | 99.000 | 0.000 |
| 5 | 110.0960 | −25.1629 | 14.618 | 14.142 | 14.054 | 13.977 | 0.017 | 0.000 | 0.000 | 13.434 | 0.085 | 0.000 | 0.000 | 99.000 | 0.000 |

**Note.** The table includes photometry for all stars on the NGC 2362 field with a detection in IRAC and/or MIPS. Values of 99.000 or 0.00 in the photometry column and 0.00 in the photometric uncertainty columns denote sources that were not observed in a given filter.
(This table is available in its entirety in a machine-readable form in the online journal. A portion is shown here for guidance regarding its form and content.)

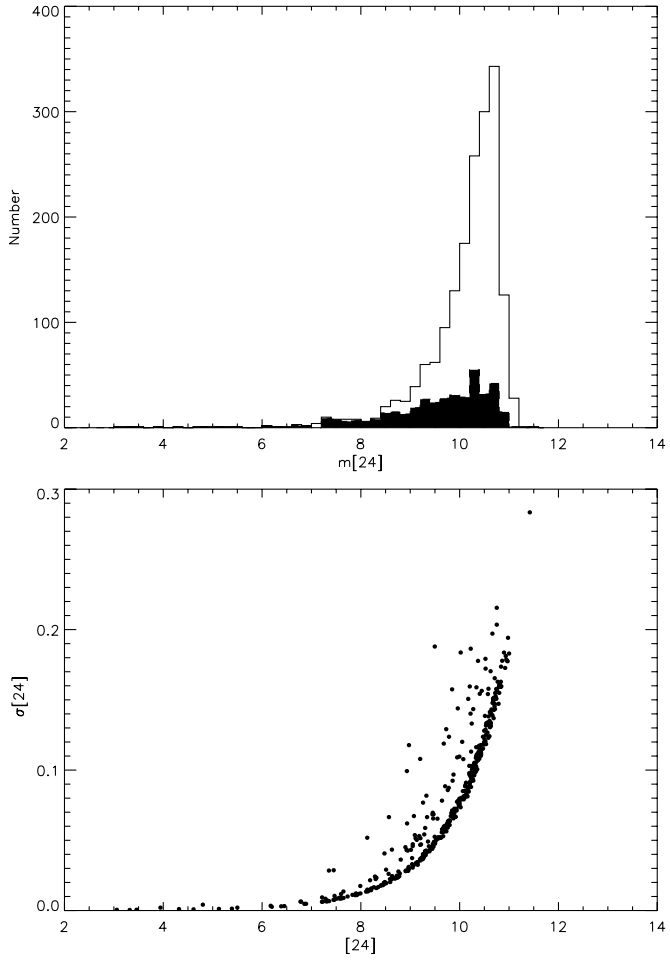


**Figure 2.** Top: histogram of MIPS 24 $\mu$m detections (solid line) and sources with 2MASS counterparts (filled region). Bottom: error distribution of 24 $\mu$m detections with 2MASS counterparts. Sources with photometric errors slightly greater than the main distribution typically lie closer to the image edges.

**Figure 3.** False-color image of NGC 2362 made with the PBCD mosaic images at 4.5 $\mu$m (blue), 8 $\mu$m (green), and 24 $\mu$m (red). The bright star $\tau$ CMa is shown near the image center.

ages $\lesssim$10 Myr (e.g., Kenyon & Hartmann 1995; Dahm 2005b; Currie et al. 2007a). Young low-mass stars are also identified as having strong Li 6708 Å absorption. Finally, optical color–magnitude diagrams (e.g., $V/V - I$) can determine the cluster locus and thus identify candidate members, especially for massive clusters (e.g., Lyra et al. 2006; Currie 2008; Currie et al. 2009; T. Currie et al. 2009, in preparation).

In this section, we describe ancillary data for NGC 2362 that identifies confirmed and candidate cluster members. We draw our primary list of confirmed and candidate members from Dahm & Hillenbrand (2007) identified by Li 6708 Å absorption, X-ray activity, $H_\alpha$ emission, and optical photometry. To this list, we add a second list of candidate members identified by deep optical photometry from Irwin et al. (2008).

#### *2.2.1. Optical Photometry and Membership List from Dahm & Hillenbrand (2007)*

Dahm & Hillenbrand (2007) list 232 members from a sample of stars with $H_\alpha$ emission, Li 6707 Å absorption, and X-ray activity. About 20% of these stars show evidence of youth from all three indicators, ≈36% have at least two indicators of youth, and nearly half (≈44%) have just one indicator. To this list, Dahm & Hillenbrand (2007) add 105 sources whose optical colors/magnitudes are consistent with colors of ∼5 Myr old stars and are thus "candidate" members. While none of these stars have detected $H_\alpha$ emission, Li absorption, or X-ray activity, many of them are too faint ($V \gtrsim 21$) to be

**Table 2**
Photometry Catalog for NGC 2362 Cluster Members

| ID | R.A. | Decl. | $V$ | $R$ | $I$ | $J$ | $H$ | $K_s$ | [3.6] | $\sigma$([3.6]) | [4.5] | $\sigma$([4.5]) | [5.8] | $\sigma$([5.8]) | [8] | $\sigma$([8]) | [24] | $\sigma$([24]) |
|---|---|---|---|---|---|---|---|---|---|---|---|---|---|---|---|---|---|---|
| 1 | 109.5817 | -24.9550 | 19.430 | 18.470 | 16.800 | 15.220 | 14.620 | 14.370 | 14.130 | 0.050 | 14.110 | 0.070 | 14.125 | 0.148 | 14.054 | 0.138 | 99.000 | 0.000 |
| 2 | 109.5905 | -24.9578 | 17.420 | 16.450 | 15.650 | 14.670 | 13.950 | 13.770 | 13.580 | 0.040 | 13.590 | 0.050 | 13.491 | 0.086 | 13.705 | 0.097 | 99.000 | 0.000 |
| 3 | 109.5909 | -24.8615 | 18.170 | 17.170 | 15.950 | 14.600 | 13.860 | 13.580 | 13.240 | 0.030 | 13.060 | 0.040 | 12.745 | 0.047 | 12.089 | 0.022 | 7.649 | 0.009 |
| 4 | 109.5942 | -25.0283 | 19.680 | 18.530 | 16.920 | 15.540 | 14.910 | 14.520 | 14.280 | 0.050 | 14.250 | 0.070 | 13.979 | 0.129 | 13.885 | 0.117 | 99.000 | 0.000 |
| 5 | 109.6002 | -24.8997 | 18.890 | 17.840 | 16.420 | 14.930 | 14.410 | 14.010 | 14.000 | 0.060 | 13.850 | 0.060 | 13.819 | 0.113 | 13.992 | 0.130 | 99.000 | 0.000 |

**Note.** The table includes photometry for NGC 2362 cluster members identified by Dahm & Hillenbrand (2007). Values of 99.000 or 0.00 in the photometry column and 0.00 in the photometric uncertainty columns denote sources that were not observed in a given filter.
(This table is available in its entirety in a machine-readable form in the online journal. A portion is shown here for guidance regarding its form and content.)

**Table 3**
Photometry Catalog for NGC 2362 Candidate Members from Irwin et al. (2008)

| ID | R.A. | Decl. | $V$ | $I$ | $J$ | $H$ | $K_s$ | [3.6] | $\sigma$([3.6]) | [4.5] | $\sigma$([4.5]) | [5.8] | $\sigma$([5.8]) | [8] | $\sigma$([8]) | [24] | $\sigma$([24]) |
|---|---|---|---|---|---|---|---|---|---|---|---|---|---|---|---|---|---|
| 1 | 109.5003 | -25.1379 | 20.515 | 17.525 | 15.985 | 15.346 | 14.938 | 14.835 | 0.030 | 14.831 | 0.041 | 14.773 | 0.265 | 14.637 | 0.273 | 99.000 | 0.000 |
| 2 | 109.5145 | −25.1769 | 16.786 | 15.526 | 14.564 | 13.971 | 13.854 | 0.000 | 0.000 | 13.793 | 0.020 | 0.000 | 0.000 | 14.005 | 0.135 | 99.000 | 0.000 |
| 3 | 109.5160 | −25.1295 | 21.548 | 18.795 | 99.000 | 99.000 | 99.000 | 16.067 | 0.079 | 16.044 | 0.111 | 0.000 | 0.000 | 0.000 | 0.000 | 99.000 | 0.000 |
| 4 | 109.5212 | −25.1615 | 20.936 | 18.074 | 16.399 | 15.728 | 99.000 | 15.392 | 0.045 | 15.228 | 0.056 | 14.925 | 0.308 | 14.879 | 0.369 | 99.000 | 0.000 |
| 5 | 109.5234 | −25.2406 | 22.386 | 18.925 | 16.617 | 15.570 | 14.916 | 0.000 | 0.000 | 0.000 | 0.000 | 0.000 | 0.000 | 0.000 | 0.000 | 9.800 | 0.064 |

**Note.** The table includes photometry for candidate NGC 2362 cluster members identified by Irwin et al. (2008). Values of 99.000 or 0.00 in the photometry column and 0.00 in the photometric uncertainty columns denote sources that were not observed in a given filter.
(This table is available in its entirety in a machine-readable form in the online journal. A portion is shown here for guidance regarding its form and content.)

studied with spectroscopy or X-ray surveys. Other stars are too early in spectral type for the nondetections of $H_\alpha$ emission, Li absorption, or X-ray activity to rule out membership.

Using a 2″ matching radius, we identify all cluster members in at least one IRAC channel and 39 cluster members with MIPS. Increasing the radius to 3″ does not yield any new MIPS matches and increases the likelihood of contamination by background galaxies. Thus, about 12% of the known cluster members are detected by MIPS: analysis of the mid-IR properties of cluster members (Section 3) is limited by many upper limits. Table 2 lists the combined optical/IR (IRAC and MIPS) photometry of members from the Dahm & Hillenbrand (2007) catalog, using IRAC photometry from this paper.

While the membership list from Dahm & Hillenbrand (2007) is robust, it is spatially limited and does not include the lowest-mass stars. The grism spectra used to identify $H_\alpha$ emitters are restricted to stars within a $11' \times 11'$ region surrounding the cluster center (near $\tau$ CMa; $\alpha = 07^{\rm h}18^{\rm m}40\overset{\rm s}{.}4$, $\delta = -24^\circ 33' 31\overset{''}{.}3$). *Chandra*/ACIS observations which detect identify X-ray active members are limited to a $16\overset{'}{.}9 \times 16\overset{'}{.}9$ area surrounding the cluster center. Finally, Dahm (2005a) identifies candidate cluster members from photometry for stars with $V \lesssim 21$ within 7′ of the cluster center.

According to Dahm (2005a), cluster members with $H_\alpha$ emission, X-ray activity, and/or Li absorption are very centrally concentrated. The surface density of members drops by a factor of 2 at a cluster radius of ≈2′ and merges with background by ≈6′–7′. However, many massive clusters (e.g., $h$ and $\chi$ Persei; Currie et al. 2007c) contain a low-density halo/distributed population of young stars located many core radii away from the cluster centers. The halo population may contain as much mass as the bound cluster population (T. Currie et al. 2009, in preparation).

### 2.2.2. *Optical Photometry and Expanded List of Candidate Members from Irwin et al. (2008)*

To identify candidates for fainter members of the cluster and members of a surrounding halo-population, we rely on the deep optical photometry of NGC 2362 from Irwin et al. (2008). As a part of the MONITOR program (Aigrain et al. 2007), Irwin et al. (2008) imaged a $36' \times 36'$ field centered on $\tau$ CMa with the MOSAIC Imager on the 4 m Blanco telescope at CTIO. The Irwin et al. catalog includes ≈56,000 stars with $5\sigma$ detections at a magnitude limit of $I \sim 23.6$.

Irwin et al. (2008) identify ∼1826 stars brighter than $V \sim 25$ whose positions on the $V/V - I$ color–magnitude diagram are consistent with cluster membership. About 1465 of these stars lie outside the Dahm (2005a) survey limits, greater than 7′ away from the NGC 2362 cluster center. All of these stars are fainter than $V \sim 16.5$.[7] Using a simulated catalog of field objects from the Besacon Galactic models (Robin et al. 2003), Irwin et al. (2008) estimate a contamination level of ∼65%, which implies that NGC 2362 contains a population of ∼600–650 faint stars, ∼500 of which lie in a halo population surrounding the cluster. Thus, the candidate member list from Irwin et al. (2008) may identify new members.

Because the Irwin et al. (2008) catalog may include cluster members, combining their source list with the MIPS detections may reveal additional cluster stars with mid-IR excess emission from disks. In total, 1143 stars from Irwin et al. (2008) have IRAC and/or MIPS counterparts and are not in the Dahm & Hillenbrand (2007) membership sample. Nearly all (1120) of these stars are located beyond the bound cluster region (⩽7′ from the cluster core). Table 3 lists the optical, 2MASS, and *Spitzer* photometry of these candidate members.

[7] Brighter stars are saturated.

## 3. 2MASS/IRAC AND MIPS COLORS OF NGC 2362 CLUSTER MEMBERS AND CANDIDATE MEMBERS

To identify disk-bearing stars in NGC 2362, we analyze the mid-IR colors of confirmed and new candidate cluster members.[8]

We use IRAC colors to identify stars with warm dust emission from the inner disk. Then we analyze MIPS colors to identify stars with colder emission. Comparing the IRAC and MIPS colors provides a first-order investigation of the NGC 2362 disk population. Comparisons between our photometry and that from Dahm & Hillenbrand (2007) are discussed in Appendix A.

### 3.1. IRAC Colors

Figures 4 and 5 show the distributions of $K_s$–[5.8] (left panels) and $K_s$–[8] (right panels) colors for NGC 2362 stars from the Dahm & Hillenbrand (2007) sample (Figure 4) and candidates from Irwin et al. (2008, Figure 5). To show how these colors vary with stellar properties, we plot them against the 2MASS $J$–$K_s$ color. For cluster stars with similar extinction, the observed $J$–$K_s$ serves as a good tracer of spectral type. Late-type K and M stars have red $J$–$K_s$ colors ($\gtrsim$0.6); early-type B and A stars have $J$–$K_s$ $\approx$0. The positions of these stars in optical color–magnitude diagrams define a tight locus (Dahm & Hillenbrand 2007; Moitinho et al. 2001), which suggests that the cluster lacks a large age spread. Therefore, the $J$–$K_s$ color also correlates well with stellar mass.

To compare the observed $K_s$–[5.8, 8] colors to predicted photospheric colors, we overplot the locus of photospheric colors (dotted lines) from the STAR-PET interactive tool available from the *Spitzer Science Center* Web site.[9] All sources with photometric uncertainties of $\leqslant$0.5 mag are shown. Sources with (without) MIPS detections are shown as black dots (triangles).

In both panels of Figure 4, the distribution of the IRAC colors follows the trends expected for a young cluster. Most sources lie within ~0.2 mag of the predicted photospheric colors, which range from $K_s$–[8] ~ 0 for early-type stars ($J$–$K_s$ ~ 0) to ~0.5–0.6 for late-type stars ($J$–$K_s$ ~ 0.8). Very few stars have $K_s$–[5.8, 8] $\lesssim$ 0. The Dahm & Hillenbrand (2007) sample lacks high-mass stars ($J$–$K_s$ $\leqslant$ 0.4) with red IRAC colors that are indicative of excess emission from warm dust. In contrast, many late-type, lower-mass stars ($J$–$K_s$ $\gtrsim$ 0.6 − $M_\star$ $\lesssim$ 1.4 $M_\odot$ at 5 Myr; Baraffe et al. 1998) show evidence for IR excess emission.

Most stars with clear IRAC excesses have MIPS detections. The MIPS-detected population (black dots) has a narrower range in $J$–$K_s$ (~0.8–1.4) than the IRAC-detected population. The IRAC colors of MIPS-detected stars also show evidence for a wavelength-dependent luminosity of disk emission. MIPS-detected stars characteristically have $K_s$–[5.8] ~ 1. The $K_s$–[8] colors for most of these stars are slightly redder ($K_s$–[8] ~ 1.25–1.75).

The distribution of IRAC colors for the Irwin et al. (2008) candidates shows similar trends (Figure 5). The dispersions in $K_s$–[5.8] and $K_s$–[8] colors are ~0.2 mag. The Irwin et al. (2008) sample shows evidence for a clear IR-excess population ($K_s$–[5.8, 8] $\gtrsim$ 0.5–0.75), which is smaller than that for the Dahm & Hillenbrand (2007) sample. MIPS-detected stars in this sample have $K_s$–[5.8] ~ 1 and $K_s$–[8] ~ 1–2.

### 3.2. $K_s$–[24] Colors and Upper Limits

Figure 6 shows the $J$ versus $K_s$–[24] and $J$–$K_s$ versus $K_s$–[24] diagrams for confirmed/candidate cluster members from Dahm & Hillenbrand (2007, top panels) and candidates from Irwin et al. (2008, bottom panels). Extinction to the cluster is low (avg. $E(B-V)$ $\approx$0.1; Balona & Laney 1996; Moitinho et al. 2001) and affects optical fluxes far more than IR fluxes (e.g., Mathis 1990). Therefore, potential 24 $\mu$m excess sources are not affected by small dispersions in the reddening of cluster stars. While the Dahm & Hillenbrand (2007) sample contains some stars with $K_s$–[24] colors consistent with stellar photospheres, the Irwin et al. (2008) sample lacks photospheric sources because it contains only faint stars.

The $K_s$–[24] colors of confirmed/candidate members indicate that NGC 2362 harbors many stars with 24 $\mu$m excess emission plausibly due to circumstellar disks. MIPS detects 13/22 of the known cluster members brighter than $J$ = 11 (Figure 6, top left panel). These bright sources have $J$–$K_s$ $\approx$0, indicative of early spectral-type stars (Figure 6, right panels). Thus, the MIPS observations probably detect photospheric emission from many early-type (B–A) cluster members. The locus of sources with 24 $\mu$m detections and upper limits in Figure 6 (left panels) shows that MIPS detects both weak ($K_s$–[24] ~ 1–3) and strong ($K_s$–[24] $\gtrsim$3–4) excesses around stars with $J$ ~ 12–14.5 and only strong excesses around fainter stars. By comparing the locus of colors as a function of $J$ magnitude and $J$–$K_s$ color, we rule out the presence of strong 24 $\mu$m emission from cluster stars with $J$ $\lesssim$ 14, $J$–$K_s$ $\lesssim$ 0.6. For a 5 Myr old cluster with negligible reddening, stars with $J$–$K_s$ $\lesssim$ 0.6 have spectral types earlier than K3 and masses greater than ~1.4 $M_\odot$ (Baraffe et al. 1998).

To summarize, the population of stars with 24 $\mu$m excesses reveals a wide range of mid-IR disk luminosities. Most bright, early-type stars have photospheric MIPS emission and thus may lack circumstellar dust. Early-type stars with MIPS excesses have weak excesses, $\approx$0.5–2 mag. Later-type stars with MIPS detections typically have strong excesses. However, sensitivity limits preclude MIPS from detecting many late-type stars with weak excesses.

The positions of several stars in Figure 6 call into question their membership status. Specifically, IDs 28 and 166, listed as members in Dahm & Hillenbrand (2007) based on X-ray activity, have $J$–$K_s$ colors indicative of late-type stars ($J$–$K_s$ ~ 0.6 and 0.8) but apparently have photospheric $K_s$–[24] colors. These stars have optical and 2MASS fluxes comparable to the earliest-type stars in the cluster and are brighter than other late-type cluster members by ~3 mag. If these stars are true pre-main-sequence members, the huge implied age spread is at odds with recent work showing that NGC 2362 likely had a single, explosive burst of star formation ~4–5 Myr ago (e.g., Mayne & Naylor 2008). These stars are probably either X-ray active foreground M stars, extremely high-mass, post-main-sequence cluster members, or extragalactic sources.

[8] No source has a galaxy contamination flag in the 2MASS Point Source Catalog, indicating that its emission overlaps with that of an extended source.

[9] STAR-PET computes the 2MASS–*Spitzer* colors based on the Kurucz–Lejeune stellar atmosphere models (e.g., Kurucz 1993; Lejeune et al. 1997). Rieke et al. (2008) show that differences in IRAC and MIPS colors between synthetic and empirical A type and solar-type photospheres are $\lesssim$0.05 mag.

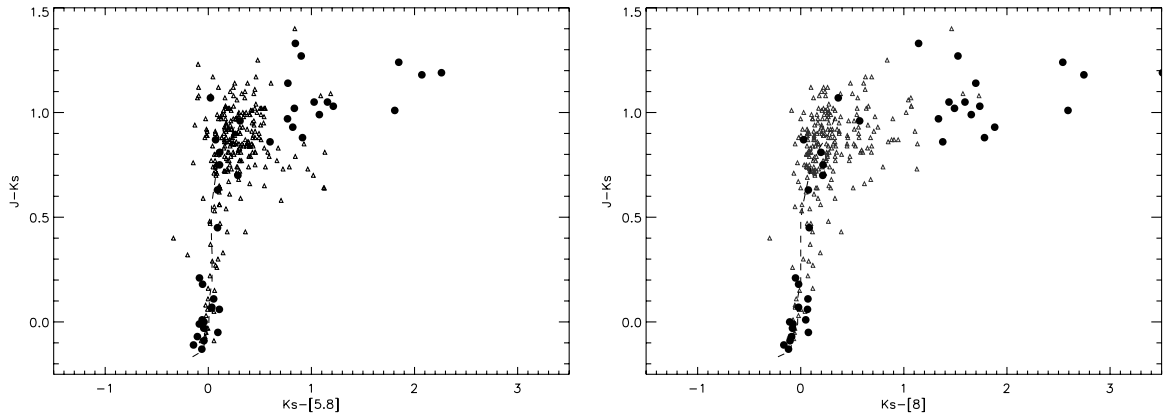


**Figure 4.** $J$–$K_s$ vs. $K_s$–[5.8] (left) and $K_s$–[8] color–color diagrams for sources in the Dahm & Hillenbrand (2007) membership list using photometry derived in this paper. Sources lacking MIPS detections are shown as triangles. Sources with MIPS detections are shown as dots. Overplotted are the loci of photospheric colors (dotted lines) from the Kurucz–Lejeune stellar atmosphere models as calculated by the SENS-PET tool. Most sources with IRAC excesses have MIPS detections.

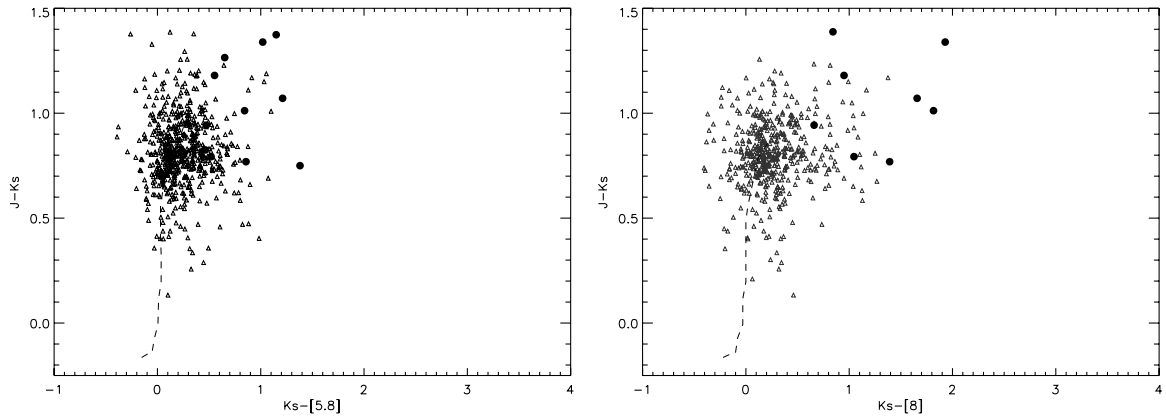


**Figure 5.** Same as Figure 4 except for the list of candidate members from Irwin et al. (2008). As with the Dahm & Hillenbrand (2007) sample, most sources with IRAC excesses have MIPS detections.

### *3.3. Combined IRAC and MIPS Colors of Cluster Members from Dahm & Hillenbrand (2007) and Candidates from Irwin et al. (2008)*

When combined with the IRAC data, the MIPS data reveal a diversity of mid-IR disk emission. Figure 7 shows the $K_s$–[5.8, 8] versus $K_s$–[24] color–color diagrams for stars in the Dahm & Hillenbrand (2007) sample (top panels) and Irwin et al. (2008) sample (bottom panels). To compare the observed colors with colors typical of primordial circumstellar disks, we overplot the colors from the median Taurus SED (Furlan et al. 2006) reddened by $E(B-V) = 0.1$. Most sources with MIPS upper limits (gray arrows) have $K_s$–[8] $\sim -0.2$–0.5. About 18 stars have $\gtrsim$3.5 mag MIPS excesses. Comparing their $K_s$–[24] colors in Figure 7 to the distribution of $K_s$–[24] colors versus $J$–$K_s$ in Figure 4 shows that all stars with strong MIPS *and* IRAC excesses are late-type, low-mass stars.

Most sources with IRAC and MIPS excess emission have weaker emission than the Taurus sources with primordial disks. Because many of the 85 Taurus sources used to construct the median SED have evidence for inner holes/gaps (e.g., DM Tau, UX Tau), stars surrounded by full primordial disks should have $K_s$–[5.8, 8] colors comparable to or greater than those for the median Taurus SED. Only four NGC 2362 sources have IRAC excesses exceeding that of the median Taurus SED. Most sources with excess emission have weaker emission than the median Taurus SED at both IRAC and MIPS wavelengths. Sources with IRAC and/or MIPS excesses weaker than the median Taurus SED, show a further diversity. Among the sources with 24 $\mu$m excesses equal to or greater than the median Taurus SED, nearly half have IRAC fluxes in at least one filter that are reduced by a factor of $\sim$2 from the median Taurus SED.

## 4. ANALYSIS OF THE NGC 2362 DISK POPULATION

The combined IRAC and MIPS photometry of confirmed/candidate cluster members reveals sources with a wide range of mid-IR excess emission consistent with a range of disk evolutionary states. In general, stars with blue $J$–$K_s$ colors ($\leqslant$0.4; early-type stars) either lack 24 $\mu$m excess emission or have weak 24 $\mu$m excess emission ($K_s$–[24] $\sim$ 0.5–2). Stars with redder ($J$–$K_s > 0.6$; late-type stars) colors have strong 24 $\mu$m excess emission ($K_s$–[24] $\sim$ 3–7) presumably from optically thick circumstellar disks. Furthermore, the combined IRAC and MIPS colors show that stars with strong 24 $\mu$m disk emission have a wide range of emission from inner disk regions probed by the IRAC 3.6–8 $\mu$m filters. The variety of mid-IR fluxes from disks surrounding NGC 2362 stars then warrants and enables detailed comparisons with predicted fluxes from disks spanning a range of evolutionary states.

In this section, we explore the NGC 2362 disk population in more detail by using models to constrain the evolutionary

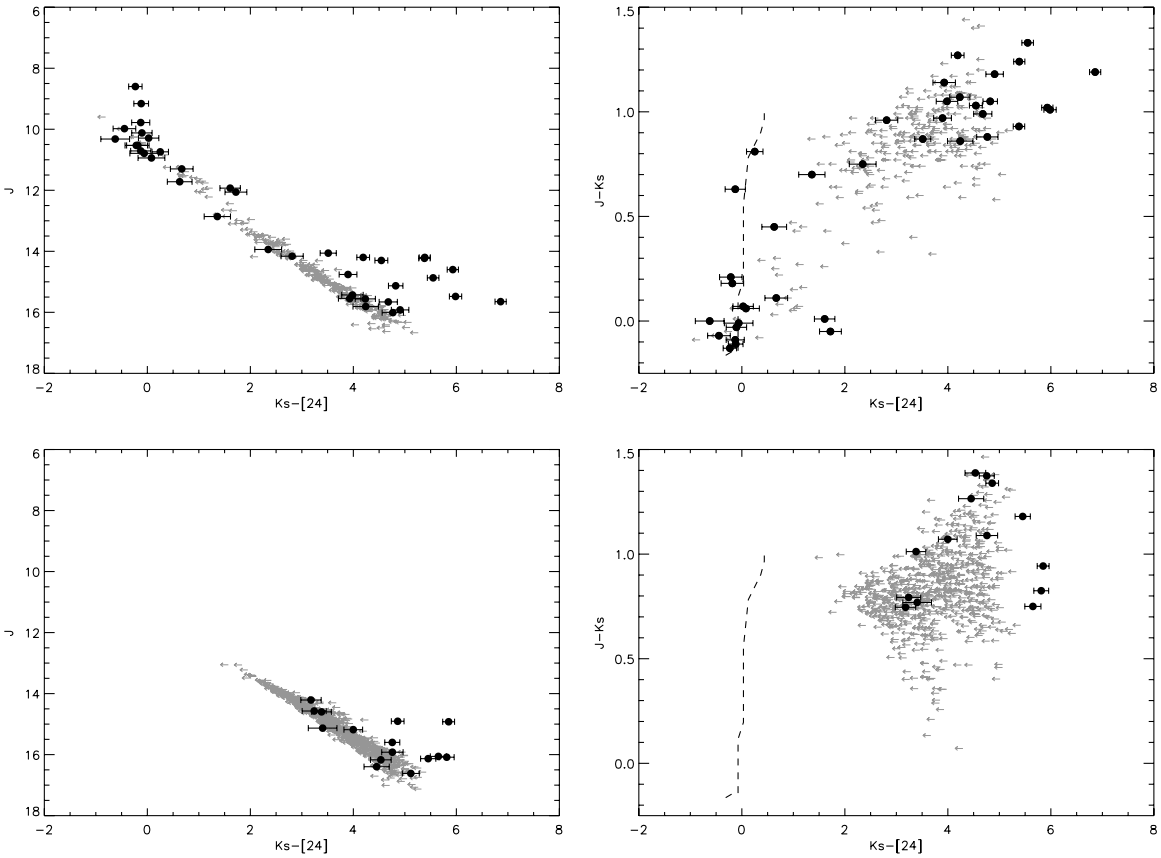


**Figure 6.** $J$ vs. $K_s$–[24] (left) and $J$–$K_s$ vs. $K_s$–[24] (right) color–color diagrams for confirmed/candidate cluster members from Dahm & Hillenbrand (2007, top) and candidates from Irwin et al. (2008, bottom). The leftward arrows identify $K_s$–[24] upper limits for sources lacking MIPS detections.

state of disks surrounding early-type, high/intermediate-mass stars and late-type, low-mass stars. By comparing the observed SEDs of early-type stars to best-match SEDs from the Robitaille et al. (2006) radiative transfer models, we estimate the mass of emitting dust needed to reproduce the observed disk emission. We then compare this dust mass to dust masses for disks in several evolutionary states and derive the dust removal timescales.

For late-type stars, our approach is twofold. First, we compare the source SEDs to the median Taurus SED and to predictions for warm debris disk emission. The median Taurus SED serves as an empirically based fiducial primordial disk model. In the debris disk model (Kenyon & Bromley 2004), debris emission from terrestrial planet formation is calculated at 0.7–2 AU from a 1 $M_\odot$ star and tracked for ∼100 Myr. The disk luminosity as a function of wavelength at 5 Myr is converted into a flux and scaled to the stellar photosphere. In these comparisons, we emphasize that no attempt is made to fit the observed SEDs. Rather, comparing the source SEDs to the median Taurus and debris disk models can constrain whether the SED is "primordial disklike," "debris disklike," or in between. For a second check on the disk evolutionary state, we fit the observed SEDs to the Robitaille et al. (2006) models to determine the allowed ranges of dust masses, inner hole sizes, and disk flaring indices using the SED fitting tool of Robitaille et al. (2007). From this analysis, we determine the relative frequency of primordial disks, debris disks, and disks in an intermediate stage surrounding late-type stars.

### *4.1. Mid-IR Disk Emission from $\gtrsim$1.4 $M_\odot$-Mass Stars*

#### *4.1.1. SED Modeling of $\gtrsim$1.4 $M_\odot$ Stars*

To model the mid-IR emission from early-type stars with 24 $\mu$m excess emission, we compare their SEDs to the grid of 200,000 radiative transfer models from Robitaille et al. (2006). The Robitaille et al. (2006) models predict the thermal emission of sources including contributions from stellar photospheres, infalling envelopes, bipolar cavities, and accreting circumstellar disks. The model parameters are varied for stars with a wide range of stellar temperatures. Dust masses are derived assuming a standard ISM size distribution ($n(a) \propto a^{-3.5}$). By selecting the best-matching SEDs, we estimate the masses of small ($\lesssim$100 $\mu$m–1 mm) dust grains that are required to reproduce the observed level of emission. We then compare these masses to typical dust masses for debris disks and primordial disks. Typical dust masses for debris disks range from $10^{-11}\,M_\odot$ to $5\times10^{-9}\,M_\odot$ (e.g., Chen et al. 2005; Low et al. 2005). Typical dust masses for primordial disks range from $10^{-5}\,M_\odot$ to $10^{-3}\,M_\odot$ (e.g., Andrews & Williams 2005). To estimate spectral types of these stars, we use their observed $J$–$K_s$ colors. We model the SEDs of the four sources—IDs 31, 144, 303, and 314—with $K_s$–[24] = 0.5–2.5.

Figure 8 shows SED model fits to the four early/intermediate-type stars with MIPS excesses, the results of which are summarized in Table 4. The best-matching Robitaille et al. (2006) models overpredict the observed fluxes from these sources at all

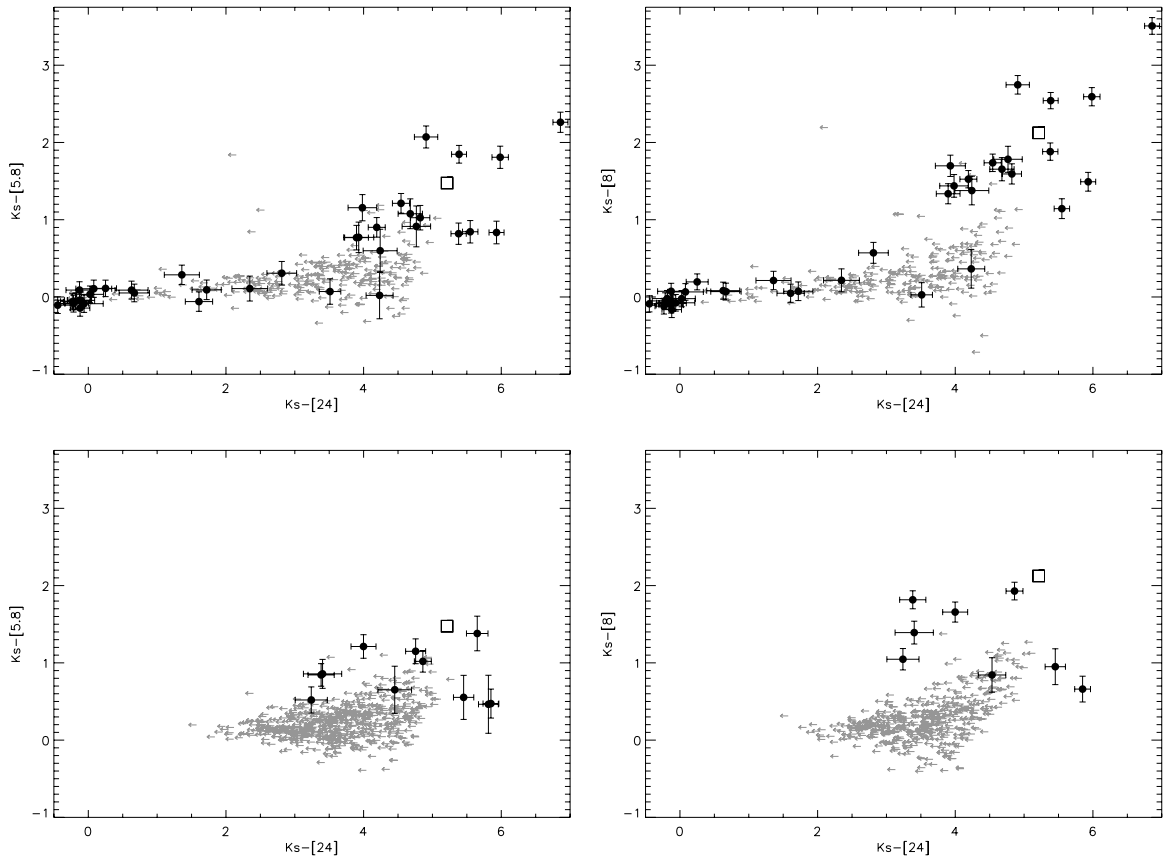


**Figure 7.** $K_s$–[5.8,8] vs. $K_s$–[24] color–color diagrams for the Dahm & Hillenbrand (2007) sample (top). Overplotted are the colors from the median Taurus SED (Furlan et al. 2006) reddened by $E(B-V) = 0.1$ (square). Top left: the $K_s$–[5.8] vs. $K_s$–[24] color–color diagram. Sources with 24 $\mu$m upper limits are shown as gray left-pointing arrows. MIPS-detected sources (black dots) are shown overplotted with 1$\sigma$ photometric errors. Top right: the $K_s$–[8] vs. $K_s$–[24] color–color diagram for Dahm & Hillenbrand sources. The symbols are the same as in the left-hand panel. Bottom: $K_s$–[5.8,8] vs. $K_s$–[24] color–color diagrams for the Irwin et al. (2008) sample.

**Table 4**
Dust Removal Timescales and Dust Masses for Early-Type Stars with MIPS 24 $\mu$m Excesses

| ID | $J$–$K_s$ | Spectral Type (Estimated) | $L_\star/L_\odot$ (Estimated) | $M/M_\odot$ (Estimated) | $r_{\rm dust}$ (AU) (200, 120 K) | $t_{\rm pr}$ (yr) (10, 30 AU) | $s_{\rm max}$ ($\mu$m) | Disk Model | max($M_{\rm dust}$) ($\times 10^{-10} M_\odot$) |
|---|---|---|---|---|---|---|---|---|---|
| 31 | 0.11 | A5 | 30.0 | 2.3 | 10.7,29.8 | $2.3 \times 10^4$, $2.1 \times 10^5$ | 14.8 | 3020154-5-9 | 14 |
| 144 | 0.45 | G5 | 10.0 | 2.0 | 6.2,17.2 | $7.0 \times 10^4$, $6.3 \times 10^5$ | 5.8 | 3008807-5-9 | 1.1 |
| 303 | 0.01 | A0 | 35.3 | 2.5 | 11.6,32.3 | $2.0 \times 10^4$, $1.8 \times 10^5$ | 16.0 | 3017274-5-9 | 2.2 |
| 314 | −0.05 | B9 | 56.5 | 2.7 | 14.7,40.9 | $1.2 \times 10^4$, $1.1 \times 10^5$ | 23.8 | 3017274-5-9 | 2.2 |

**Note.** Constraints on the dust removal timescales and dust masses for early-type sources. The Poynting–Robertson drag timescale is calculated assuming 10 $\mu$m sized grains. Disk models listed represent the file number from the Robitaille et al. (2006) grid; dust masses for those models are listed as $M_{\rm dust}$.

mid-IR wavelengths,[10] which indicates that the dust masses required to reproduce the observed disk emission through 24 $\mu$m are considerably less than the fitted masses. Three of the four sources—IDs 144, 303, and 314—have significant 24 $\mu$m excesses above the model stellar photosphere (dotted line). The 24 $\mu$m flux from ID 31 lies just barely above the photosphere ($(K_s$–[24])/$\sigma$([24]) ≈4) so this source has marginal evidence for a disk. The dust masses for the best-fit Robitaille et al. models are ∼1–10 × $10^{-10}$ $M_\odot$, or ∼7 orders of magnitude less than typical masses of dust in primordial disks. Unless these sources have enormous reservoirs of extremely cold dust, which would not contribute significantly to the observed 24 $\mu$m emission, the total mass of dust in small grains is likely small compared to primordial dust masses as well. The extremely low required dust masses required imply that the disks are optically thin through 24 $\mu$m. These dust masses are inconsistent with masses typical of primordial disks but are consistent with debris disk masses (e.g., Chen et al. 2006).

#### *4.1.2. Dust Dynamics in Disks Surrounding $\gtrsim$1.4 $M_\odot$ Stars*

Next, we use dynamical arguments to show that, that dust surrounding high/intermediate-mass stars is most likely from debris disks (Table 4). In optically thin conditions, small dust grains are removed from the circumstellar environment by

[10] Even though the "fits" are obviously poor and clearly overestimate the mass of dust required to reproduce the observed emission, the Robitaille et al. (2006) grid lacks SEDs for disks with lower dust masses. Therefore, these are technically the "best-fit" models.

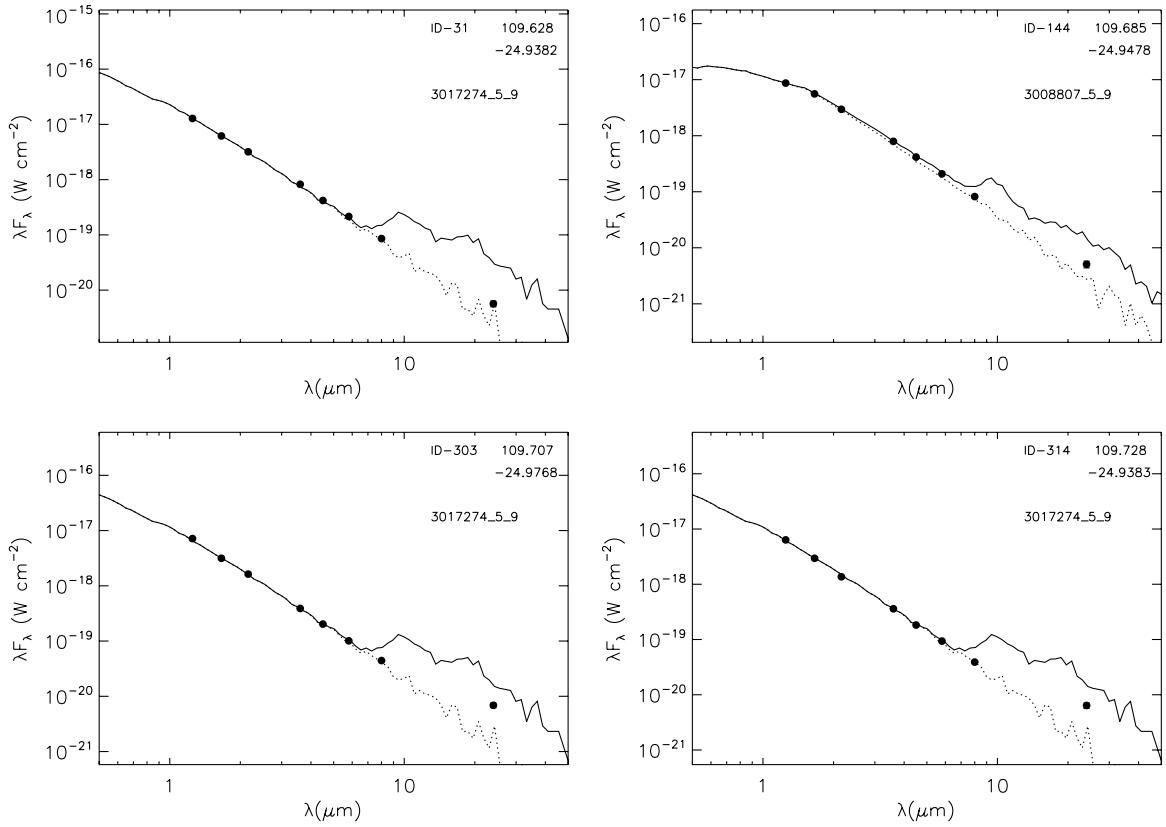


**Figure 8.** SEDs of early/intermediate-type stars with masses $\gtrsim$1.4 $M_\odot$. Overplotted are the best-fitting SEDs from Robitaille et al. (2006, solid line) along with the stellar photosphere (dotted line). Also listed is the J2000 source position (in degrees). Photometric uncertainties are smaller than the symbol sizes. Inferred dust masses are $10^{-10}$ $M_\odot$ to $10^{-9}$ $M_\odot$, consistent with debris disks.

Poynting–Robertson drag and radiation pressure. The timescale for dust removal by Poynting–Robertson drag is (e.g., Backman & Paresce 1993; Augereau et al. 1999)

$$t_{\rm P-R}({\rm yr}) \sim 705 \frac{\rho_s L_\odot}{\langle Q_{\rm abs}\rangle L_\star} s_{\mu{\rm m}} r_{\rm AU}^2, \quad (1)$$

where $r_{\rm AU}$ is the distance from the central star, $s$ is the radius of the grain, $\rho_s$ is the grain volume density, and $\langle Q_{\rm abs}\rangle$ is the absorption coefficient.

To derive the drag timescale for grains in the NGC 2362 sources, we consider typical parameters for $r_{\rm AU}$, $\langle Q_{\rm abs}\rangle$, and $\rho_s$. These sources have negligible 8 $\mu$m excesses but clear 24 $\mu$m excesses. Thus, the typical grain temperature is likely $\approx$100–200 K. For grains in radiative equilibrium, $r_{\rm AU}\sim(L_\star/L_\odot)^{0.5}$ $(T/280\,{\rm K})^{-2}$. Assuming an age of 5 Myr, early- and intermediate-type stars in NGC 2362 have luminosities $\sim$10–56 $L_\odot$ (Siess et al. 2000). Therefore, $r \sim$ 6–40 AU for $T \sim$ 100–200 K. We adopt $r \sim$ 10–30 AU, roughly the mean distances for 200 K and 120 K dust in our sample. For grains with $\rho_s \sim 1$ g cm$^{-3}$ and $\langle Q_{\rm abs}\rangle \sim 1$ (Burns et al. 1979)

$$t_{\rm P-R}({\rm yr}) \sim 7\times10^4 \left(\frac{L_\odot}{L_\star}\right)\left(\frac{s}{1\mu{\rm m}}\right)\left(\frac{r}{10{\rm AU}}\right)^2. \quad (2)$$

For these massive stars, P–R drag removes small grains on timescales shorter than the $\sim$5 Myr age of sources in NGC 2362. For 10 $\mu$m grains orbiting stars with $L_\star\sim$10–56 $L_\odot$, the drag time is $t_{\rm P-R}\lesssim 6.3\times10^5$ yr. Grains with s $\lesssim$10 $\mu$m are probably porous, with $\rho_s\sim$ 0.1 g cm$^{-3}$ instead of our adopted $\rho_s\sim$ 1 g cm$^{-3}$ (e.g., Augereau et al. 1999). Porous grains have very short lifetimes, $t_{\rm P-R} \lesssim 6.3\times10^4$ yr. Thus, our derived upper limit for $t_{\rm P-R}$ is conservative.

If the ratio of the force from radiation pressure to gravity ($\beta$) exceeds 1/2,[11] radiation pressure can remove smaller grains on faster, dynamical timescales (e.g., Burns et al. 1979; Strubbe & Chiang 2006):

$$\beta_{\rm pr} = \frac{3L_\star\langle Q_{\rm pr}(a)\rangle}{16\pi G M_\star c s \rho_s} > 1/2. \quad (3)$$

This equation can be rearranged to solve for the grain size below which radiation pressure can remove dust from the system (Burns et al. 1979; Backman & Paresce 1993):

$$s_{{\rm max},\mu{\rm m}} < 1.14\ \mu{\rm m}\left(\frac{L_\star}{L_\odot}\right)\left(\frac{M_\odot}{M_\star}\right)\left(\frac{1\,{\rm g\,cm^{-3}}}{\rho_s}\right)\langle Q_{\rm pr}\rangle. \quad (4)$$

For stars listed in Table 4, $s_{\rm max}$ ranges from 5.8 to 23.8 $\mu$m, assuming $\langle Q_{\rm pr}\rangle \approx 1$ and $\rho_s \approx 1$ g cm$^{-3}$. Using a more realistic dust grain porosity makes even more grains subject to blowout by radiation pressure. Therefore, grains responsible for producing the observed 24 $\mu$m emission should be blown out unless they are replenished by collisions between larger bodies.

As long as the gas density is low, radiation pressure can remove small grains on short timescales. When the grains are poorly coupled to the gas, radiation removes grains

[11] Strubbe & Chiang (2006) argue that grains more easily become unbound, on a dynamical timescale once $\beta > 1/2$, not 1.

on timescales comparable to the local dynamical timescale, $\lesssim 10^3$ yr. In gas disks with $M_{\rm gas} \sim 1$–$10\ M_\oplus$, small ($\lesssim$10–50 $\mu$m) dust grains are well coupled to the gas. Even in these circumstances, they are pushed by radiation pressure from $\approx$10 AU to hundreds of AU in $\approx 10^4$ yr if the disk is optically thin (Takeuchi & Artymowicz 2001). Disk emission originating at tens of AU then requires an active replenishment source and thus is likely second generation.

The properties of disks surrounding early-type NGC 2362 stars are highly suggestive of debris disks (Backman & Paresce 1993). The small IR excesses in dusts imply that the disks have very low luminosities compared to their stars and have a low mass in dust. The rapid removal timescales for this dust, regardless of whether there exists residual gas, indicates that the dust is likely second generation. Disks with copious amounts of circumstellar gas almost without exception have much stronger broadband near-to-mid-IR disk emission than that observed here. Thus, all known observed and inferred disk properties fit standard debris disk characteristics and not primordial disk characteristics. More sensitive measures of circumstellar gas (e.g., optical echelle spectroscopy) would provide an even better test of our conclusion that these disks are debris disks.

### *4.2. SEDs of Solar/Subsolar-Mass Stars*

Appendix B shows the atlas of SEDs for all late-type (candidate) cluster members from Dahm & Hillenbrand (2007) and Irwin et al. (2008) with $K_s$–[24] $\gtrsim$1. The two late-type stars in Dahm & Hillenbrand (2007) with questionable membership status lack disk emission and are not shown.

In each panel, we overplot the 1$\sigma$ error bars for IRAC and MIPS data. For the stars with spectral types from Dahm (2005a), we overplot the SED of the stellar photosphere (solid line/squares) using a model specific to the spectral type. We calculate the range in reddening and extinction from comparing the observed $V - I$ colors to intrinsic colors from Kenyon & Hartmann (1995), assuming a one-subclass uncertainty in the spectral type. All but five sources have a range of extinctions consistent with $E(B-V) \sim 0.1$ (Moitinho et al. 2001). For these five sources, we use a value for reddening halfway in between the minimum and maximum $A_V$ values allowed. For the other stars with spectral types, we assume $A_v = 0.31$, which is the mean extinction to the cluster (Moitinho et al. 2001). For the stars without known spectral types, we fit the source SEDs from $I$ through $K$ band with stellar photospheres to determine the best-fit spectral type, using colors from Kenyon & Hartmann (1995) and assuming a reddening of $E(B-V) = 0.1$ ($A_v \sim 0.31$).

Because most Taurus sources lack clear $J$-band excess emission (Furlan et al. 2006), we scale the median Taurus SED (dotted line) by its $J$-band flux, setting it equal to the stellar photosphere. The median Taurus SED clearly has the strongest disk emission. The warm debris disk models (dashed line/crosses) have weaker disk emission at all mid-IR wavelengths, slightly in excess of the stellar photosphere. The nominal MIPS 24 $\mu$m detection limit in $\lambda F_\lambda$ space is overplotted as a gray dashed line ($\lambda F_\lambda \sim 5.75 \times 10^{-21}$ W cm$^{-2}$).

To compare the inferred physical states of disks with more simple empirical classifications, we measure the IRAC [3.6]–[8] flux slope for each star. We divide the sample according to the three empirical divisions from Lada et al. (2006). We label sources with $\alpha \geqslant -1.8$ as those with "strong IRAC" emission, those with $\alpha = -2.56$ to $-1.8$ as having "weak IRAC" emission, and those with $\alpha < -2.56$ as those with "photospheric" emission. Dahm & Hillenbrand (2007) use this flux slope to infer the physical structure of the disk, specifically identifying sources with $\alpha \geqslant -1.8$ as having primordial disks. Comparing the empirical disk classifications with evolutionary states determined from SED modeling allows us to compare our results with Dahm & Hillenbrand's and test the utility of using a single IRAC slope to probe disk states.

Table 5 summarizes our results and is divided into three samples: MIPS-detected sources from the Dahm & Hillenbrand (2007), MIPS-detected sources from the Irwin et al. (2008) sample, and sources lacking clear MIPS detections that have disk emission according to Dahm & Hillenbrand (2007). We list basic sources parameters (spectral type, extinction) as well as derived disk parameters—disk mass, minimum inner disk radius, and flaring index ($\beta$)—using the Robitaille et al. (2006) models which, along with comparisons to the Taurus SED and debris disk SED, determine the disk evolutionary state (e.g., Robitaille et al. 2007). For each source, we consider all models which satisfy the goodness-of-fit criterion $\chi^2 - \chi^2_{\rm best} < n_{\rm data}$ rather than simply the best-fit model. The derived disk evolutionary states for each sample are discussed in the next two sections. For the simple comparisons to the Taurus and debris disk SED, we assume a single extinction. The extinction is treated as a free parameter in the Robitaille et al. (2006) models. However, the derived evolutionary states are insensitive to changes in the assumed extinction over the range of plausible values.

#### *4.2.1. SEDs of Confirmed/Candidate Cluster Members with MIPS Detections*

The SEDs of MIPS-detected sources shown in Appendix B reveal disks with a variety of morphologies. Figure 9 shows comparisons between the Taurus and debris disk SEDs with four representative SEDs from the atlas illustrating the range of evolutionary states listed in Table 5. Figure 10 shows modeling results for one SED (ID 267) using the Robitaille et al. (2006) models. Below, we describe the characteristics for each evolutionary state and discuss their relative frequencies.

1. *Primordial Disks*—Four stars in the Dahm & Hillenbrand (2007) sample (IDs 111, 137, 139, 202) and two stars in the Irwin et al. (2008) sample (ID-IR526 and ID-IR1046) likely harbor primordial disks. These sources typically have near-to-mid IR fluxes comparable to the median Taurus SED, though ID 202 appears to have a slight near-IR flux deficit. Only one of the six sources has an SED with mid-IR clearly stronger than the median Taurus SED (ID 137). Its stronger emission may be due to a greater level of disk flaring or inclination. Comparisons with the Robitaille et al. (2006) models show that these disks probably do not have inner holes and most have masses of $M_{\rm disk}/M_\odot \sim 10^{-1}$–$10^{-2.5}$ for a solar gas-to-dust ratio, comparable to both the Minimum Mass Solar Nebula and the typical masses of primordial disks in Taurus as derived from submillimeter data (Andrews & Williams 2005).
2. *Homologously Depleted Disks*—Many stars in both the Dahm & Hillenbrand (2007) sample (12 stars) and Irwin et al. (2008) sample (five stars) show evidence for a disk that is significantly depleted in small dust grains through 24 $\mu$m relative to typical primordial disks: a "homologously depleted" disk. Like the median Taurus SED, the SED slopes for these sources typically follow a nearly power-law decline with wavelength through 24 $\mu$m. However, these sources typically show a flux deficit in the IRAC and MIPS bands relative to the median Taurus SED. Indeed, they are underluminous by a factor of >2–3 from 5.8 $\mu$m

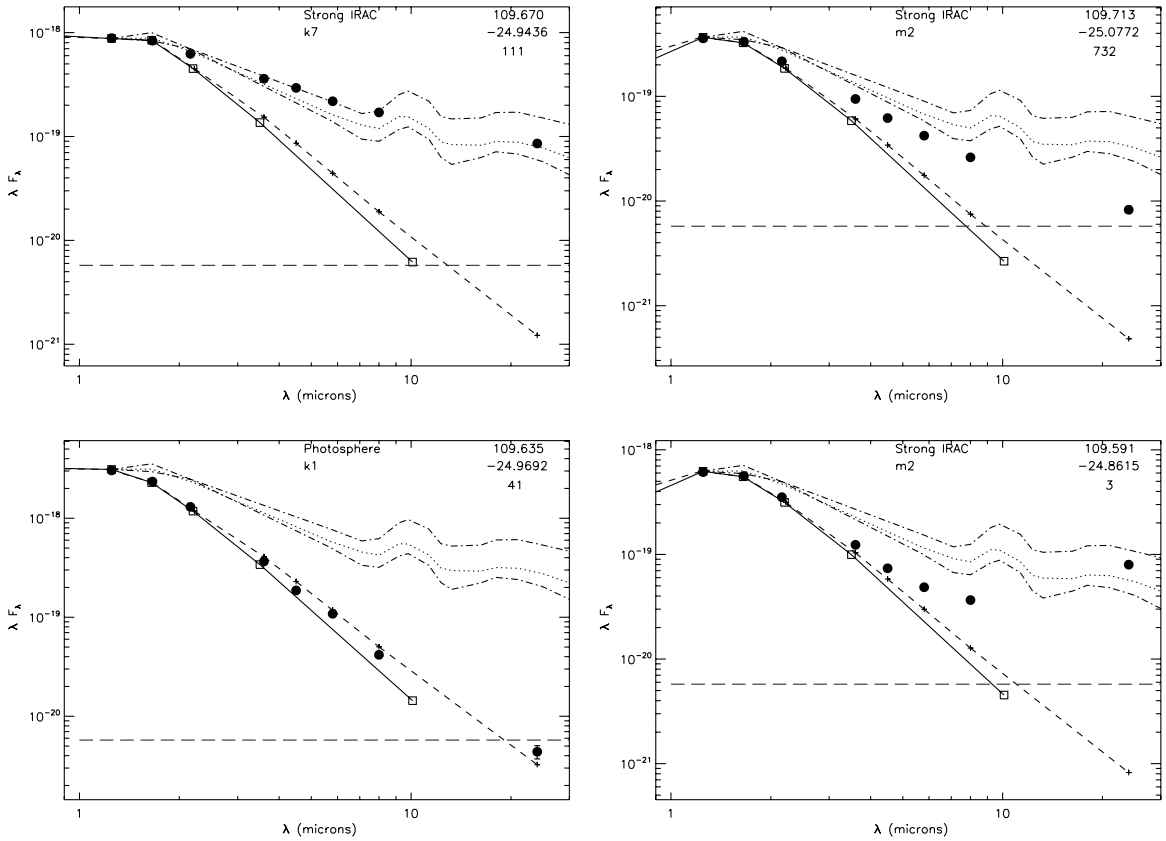


**Figure 9.** Representative SEDs of late-type NGC 2362 members and candidate members with MIPS 24 $\mu$m excesses illustrating the range of disk evolutionary states. Overplotted are the median Taurus SED (dotted line) with upper and lower quartiles (dot-dashed line). A terrestrial zone debris disk model is shown as a dashed line with mid-IR flux slightly greater than the photosphere (solid line, connected by open squares). The MIPS 5$\sigma$ detection limit is shown as a horizontal gray dashed line. The derived disk evolutionary states are (clockwise from the top left) primordial, homologously depleted, transition, and debris.

to 24 $\mu$m. Thus, they have a steeper power-law decline of disk emission with wavelength compared to primordial disks: $\lambda F_\lambda \propto \lambda^{-n}$ where $n = -7/4$ to $-5/4$. These disks also lack inner holes but have dust masses in small grains that are ∼100–1000 times less massive than their primordial disk counterparts. The dust masses in small grains required to reproduce the observed SEDs are 100–1000 times less than those of their primordial disk counterparts. They also often have little flaring (with a flaring parameter, $\beta$, of ∼1–1.1), which is consistent with a significant amount of dust settling. These features are consistent with a disk that loses a significant amount of mass of small dust grains at all disk radii simultaneously (e.g., Wood et al. 2002), which could plausibly be due to the growth of dust to larger, 1 mm–1 km-sized bodies and/or accretion onto the star.

3. *Transition Disks*—Five stars in the Dahm & Hillenbrand (2007) sample and seven stars in the Irwin et al. (2008) sample have SEDs consistent with the presence of inner holes/gaps indicative of so-called transition disks. Compared to the median Taurus SED, these sources have weaker IRAC fluxes but comparable MIPS 24 $\mu$m fluxes, a feature typical of disks with inner holes/gaps such as DM Tau, Hen 3-600A, and TW Hya (Calvet et al. 2005; Low et al. 2005). The Robitaille et al. (2006) models that provide a good fit have minimum inner holes ranging in size between 2.6 AU and 7.1 AU. Their dust masses range between $\sim 10^{-5}\,M_\odot$ and $10^{-7}\,M_\odot$. For a solar gas-to-dust ratio, the inferred disk masses range between $\sim 10^{-3}\,M_\odot$ and $\sim 10^{-5}\,M_\odot$. These values indicate that the disks are slightly depleted relative to primordial disks. One source (ID 194) has strong $K$ band and 24 $\mu$m excesses but weak IRAC excesses. Its SED may be suggestive of a disk gap instead of an inner hole.

While most sources have SEDs that are straightforward to classify, several have characteristics that make them slightly more ambiguous. Several sources (IDs 41, 63, and 196) have photospheric emission shortward of 5.8 $\mu$m or 8 $\mu$m; their 24 $\mu$m excess emission is much weaker than other late-type stars detected by MIPS ($K_s$–[24] ∼ 0.75–2.5). In this sense, their disks are consistent with being debris disks. However, dust grain removal processes (e.g., Poynting–Robertson drag) likely operate on far longer (∼1 Myr) timescales in disks surrounding these stars than disks surrounding high and intermediate-mass stars examined in Section 4.1.1. Therefore, that dust in disks surrounding these stars need not be second generation debris dust. Based on their dust masses and presence/absence of inner holes, we classify these sources as either homologously depleted disks or transition disks instead. Identifying these sources as having debris disks changes the disks statistics we discuss later but will not qualitatively change our results.

Most (15/21) of the Dahm & Hillenbrand (2007) sample with large MIPS excesses have measured $H_\alpha$ equivalent widths. Because $H_\alpha$ emission can be due to circumstellar gas accretion, its presence also provides some constraints on disk evolutionary states. Using the results of Dahm & Hillenbrand (2007) and the criteria of White & Basri (2003) to identify accretors, two of the three sources with primordial disks and $H_\alpha$ measurements

**Table 5**
Evolutionary State of Confirmed/Candidate NGC 2362 Members with Evidence for Disk Emission

| ID | ST | $A_v$ Range | EW($H_\alpha$) | $\log(M_{\rm disk}/M_\odot)$ | $R_{\rm in,min}$ (AU) | $\beta$ | Disk Type | Notes |
|---|---|---|---|---|---|---|---|---|
| Dahm & Hillenbrand (2007) sample with MIPS detections | | | | | | | | |
| 3 | M2 | 0–0.65 | NA | −4.51 ± 0.48 | 4.10 | 1.05 | Transition | |
| 36 | K5 | 0–0.53 | −6.7 | −3.02 ± 1.06 | 0.07 | 1.02 | Homologously Depleted | |
| 41 | K1 | 0–0.33 | −0.1 | −7.39 ± 0.42 | 0.12 | 1.05 | Homologously Depleted | |
| 63 | M0[1] | 0.31? | −2.9 | −6.62 ± 1.02 | 0.06 | 1.06 | Homologously Depleted | |
| 85 | M2 | 0–0.93 | −45.4 | −3.57 ± 0.93 | 0.02 | 1.14 | Homologously Depleted | |
| 111 | K7 | 0–0.45 | −18.8 | −2.07 ± 0.36 | 0.08 | 1.13 | Primordial | |
| 139 | M2 | 0–0.8 | NA | −2.09 ± 0.39 | 0.11 | 1.13 | Primordial | |
| 168 | K3 | 0.55–0.9 | −0.2 | −5.63 ± 0.85 | 5.20 | 1.09 | Transition | |
| 177 | M2 | 0–0.2 | −3.0 | −3.12 ± 0.97 | 0.06 | 1.11 | Homologously Depleted | |
| 187 | M2 | 0.03–1.3 | −117.7 | −3.58 ± 0.7 | 0.27 | 1.04 | Primordial[2] | |
| 194 | K5 | 1.02–1.8 | −27.5 | −3.91 ± 0.57 | 7.57 | 1.12 | Transition | |
| 196 | M0[1] | 0.31? | NA | −5.95 ± 0.54 | 3.63 | 1.04 | Transition | |
| 202 | M3 | 0–1.08 | −2.6 | −2.41 ± 0.12 | 0.03 | 1.18 | Primordial | |
| 204 | M3 | 0–1.05 | −10.4 | −3.87 ± 0.85 | 0.03 | 1.16 | Homologously Depleted | |
| 213 | M3 | 0–0.8 | −10.2 | −4.35 ± 1.03 | 0.04 | 1.10 | Homologously Depleted | |
| 214 | K7 | 0–0.43 | −3.5 | −3.63 ± 1.00 | 0.06 | 1.10 | Homologously Depleted | |
| 219 | M0 | 0.78–1.68 | −5.9 | −4.24 ± 1.14 | 0.03 | 1.07 | Homologously Depleted | |
| 229 | M1.5 | 0–0.95 | −3.8 | −3.81 ± 1.05 | 0.03 | 1.07 | Homologously Depleted | |
| 251 | M2[1] | 0.31? | NA | −3.98 ± 0.82 | 0.02 | 1.15 | Homologously Depleted | |
| 267 | M2[1] | 0.31? | NA | −4.35 ± 0.79 | 0.02 | 1.12 | Homlogously Depleted | |
| 295 | M2[1] | 0.31? | NA | −4.36 ± 1.12 | 1.29 | 1.08 | Transition | |
| Irwin et al. (2008) sample with MIPS detections | | | | | | | | |
| IR-185 | M2[1] | 0.31? | NA | −4.12 ± 1.05 | 0.75 | 1.07 | Transition | |
| IR-459 | M2[1] | 0.31? | NA | −4.59 ± 1.57 | 0.05 | 1.06 | Homologously Depleted | |
| IR-526 | M2[1] | 0.31? | NA | −3.62 ± 0.76 | 0.03 | 1.14 | Primordial | |
| IR-583 | M2[1] | 0.31? | NA | −3.77 ± 0.94 | 0.6 | 1.12 | Transition | |
| IR-663 | M2[1] | 0.31? | NA | −4.41 ± 0.93 | 0.02 | 1.10 | Homologously Depleted | |
| IR-732 | M2[1] | 0.31? | NA | −3.30 ± 1.27 | 0.04 | 1.05 | Homologously Depleted | |
| IR-750 | M2[1] | 0.31? | NA | −3.10 ± 0.72 | 4.32 | 1.09 | Transition | |
| IR-809 | M2[1] | 0.31? | NA | −4.93 ± 1.07 | 0.03 | 1.08 | Homologously Depleted | |
| IR-817 | M2[1] | 0.31? | NA | −3.22 ± 0.63 | 1.95 | 1.11 | Transition | |
| IR-851 | M2[1] | 0.31? | NA | −3.25 ± 0.51 | 0.21 | 1.14 | Transition | |
| IR-931 | M2[1] | 0.31? | NA | −4.24 ± 1.27 | 0.39 | 1.03 | Transition | |
| IR-958 | M2[1] | 0.31? | NA | −5.09 ± 1.19 | 0.04 | 1.07 | Homologously Depleted | |
| IR-1046 | M2[1] | 0.31? | NA | − 2.9 ± 0.95 | 0.04 | 1.13 | Primordial | |
| IR-1091 | M2[1] | 0.31? | NA | −4.39 ± 1.64 | 1.45 | 1.06 | Transition | |
| Disk Candidates from Dahm & Hillenbrand (2007) without MIPS detections | | | | | | | | |
| 12 | M3 | 0.9–1.72 | −20.2 | ··· | ··· | ··· | Homologously Depleted | 3 |
| 27 | M3 | 0.2–1.03 | −7.2 | ··· | ··· | ··· | Homologously Depleted | 3 |
| 39 | M2[1] | 0.31? | NA | ··· | ··· | ··· | Homologously Depleted | 3 |
| 100 | K5 | 0.3–1.1 | NA | ··· | ··· | ··· | Primordial | 4 |
| 227 | M2[1] | 0.31? | <0 | ··· | ··· | ··· | Homologously Depleted | 3 |

**Notes.** Footnote (1) identifies stars whose spectral types are estimated from optical/near-IR colors. Footnote (2): IDs 187 and IR-526 have low disk masses but are classified as primordial based on their mid-IR fluxes (compared to the median Taurus SED). Note (3) in the last column—Stars with probable 2–3$\sigma$ detections at MIPS 24 $\mu$m. Note (4) in the last column—MIPS detection is blended with another star. The range in extinction, $A_v$, is calculated by comparing the observed $V-I$ colors to intrinsic colors from Kenyon & Hartmann (1995), assuming a 1 subclass uncertainty in the spectral type. Negative values for EW($H_\alpha$) identify stars with $H_\alpha$ emission. Sources lacking a measured EW($H_\alpha$) have NA listed in the EW($H_\alpha$) column. The column $\log(M_{\rm disk}/M_\odot)$ refers to the unweighted average and standard deviation of all models that provide a good fit; $R_{\rm in,min}$ is the minimum inner radius of all models with good fits.

show evidence for strong $H_\alpha$ emission and thus are accreting. None of the sources with extremely low disk masses (IDs 41, 63, and 196) show this accretion signature. Stars surrounded by transition disks and homologously depleted disks include both accretors and those lacking evidence for accretion. Not all sources have optical spectra, so it is difficult to make definitive statements about the relative frequency of accretion for each disk state. However, the lack of evidence for accretion for the sources with the weakest disk emission is consistent with a depleted reservoir of circumstellar gas in these systems. The low frequency of accretion for homologously depleted disks (20%) and their low mean $H_\alpha$ equivalent widths (mean value is 9.2 Å) is expected if these systems have lower rates of accretion and are generally more evolved than their primordial disk counterparts.

#### *4.2.2. Disk-Bearing Stars in NGC 2362 Lacking MIPS Detections*

Dahm & Hillenbrand (2007) identify 14 stars with strong IRAC-excess emission and 33 with weak IRAC-excess emission. MIPS detects 16 stars included in the Dahm & Hillenbrand (2007) list, leaving 31 without detections. Of the sources lacking

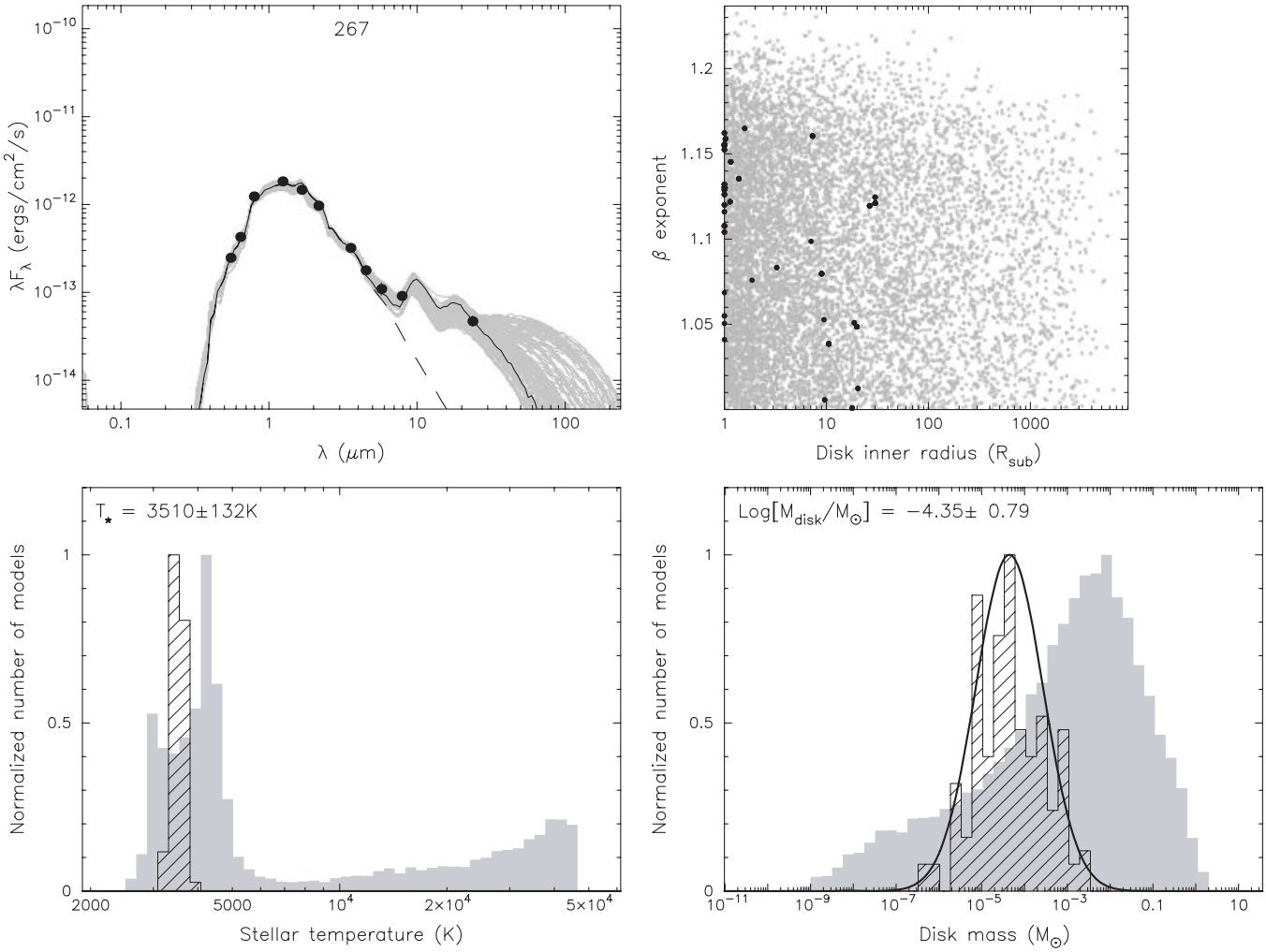


**Figure 10.** SED analysis of ID-267 using the Robitaille et al. (2006) models to fit the observed optical/IR flux (top left), constrain the inner disk radius and flaring index $\beta$ (top right), constrain the stellar temperature (bottom left), and constrain the disk mass (bottom right). The solid line in the top left plots shows the best-fitting SEDs from the Robitaille et al. grid with other possible models overplotted as faint, gray lines. In the plot of $\beta$ vs. $R_{\rm in}$ (top right panel), black dots denote the flaring index and inner disk size (in units of the sublimation radius) for the models shown in the top left panel. The gray dots show values for the entire grid. The black curves in the bottom panels define the mean and standard deviation of the stellar temperature and disk masses from the best-fitting models, the latter assuming a gas-to-dust ratio of 100. The hatched regions show the actual disk masses for each SED model shown the top left panel. The distributions of temperatures and disk masses for the entire grid are shown in gray.

MIPS detections, three have strong IRAC excesses and are classified as "primordial" by Dahm & Hillenbrand (2007);[12] Dahm & Hillenbrand classify the remaining 28 sources as "weak." Disk candidates without MIPS detections (1) could have 24 $\mu$m fluxes fainter than the MIPS detection limit, (2) could be close to a bright 24 $\mu$m source, or (3) might not be true disk-bearing stars.

To infer the physical state of disks surrounding stars without MIPS detections, we first examine the processed MIPS mosaic image to identify any stars that are $\sim$2–3$\sigma$ above the background or are blended with another star. Next, we identify stars that are accreting and thus either have primordial or more evolved primordial disks (transition/homologously depleted). Finally, we use the MIPS upper limits to constrain the possible range of 24 $\mu$m fluxes and thus constrain the disk evolutionary state.

The bottom section of Table 5 lists the results of our analysis and Figure 11 shows SEDs of five additional primordial and evolved primordial disk candidates. One star, ID 100, is likely surrounded by a primordial disk given its strong IRAC excess emission. In the MIPS 24 $\mu$m filter, it appears to be blended with a brighter cluster member. Four stars—IDs 12, 27, 39, and 227—have clear IRAC excess emission and are barely discernable on the MIPS mosaic at very high contrast. The S/N for these sources is likely $\sim$2–3, which would exclude them from the MIPS source list. ID 12 shows evidence for accretion. The SEDs of these four stars lie below the lower quartile for the median Taurus SED, which indicates that they are probably most similar to homologously depleted disks. The remaining sources lack evidence for accretion, are not discernable on the MIPS mosaic, and have weak, $\lesssim$1 mag IRAC excesses. These sources either not are true disk candidates, have very large inner holes, or harbor optically thin disks, possibly debris disks.

[12] Dahm & Hillenbrand (2007) classify disks as "primordial" or "weak" according to their IRAC flux slopes. Thus, these classifications are empirical classifications. The division between classes follows that of Lada et al. (2006). Usage of the term "primordial" in this paper always refers to the inferred *physical* state of the disk from comparing its emission to disk models and the median Taurus SED.

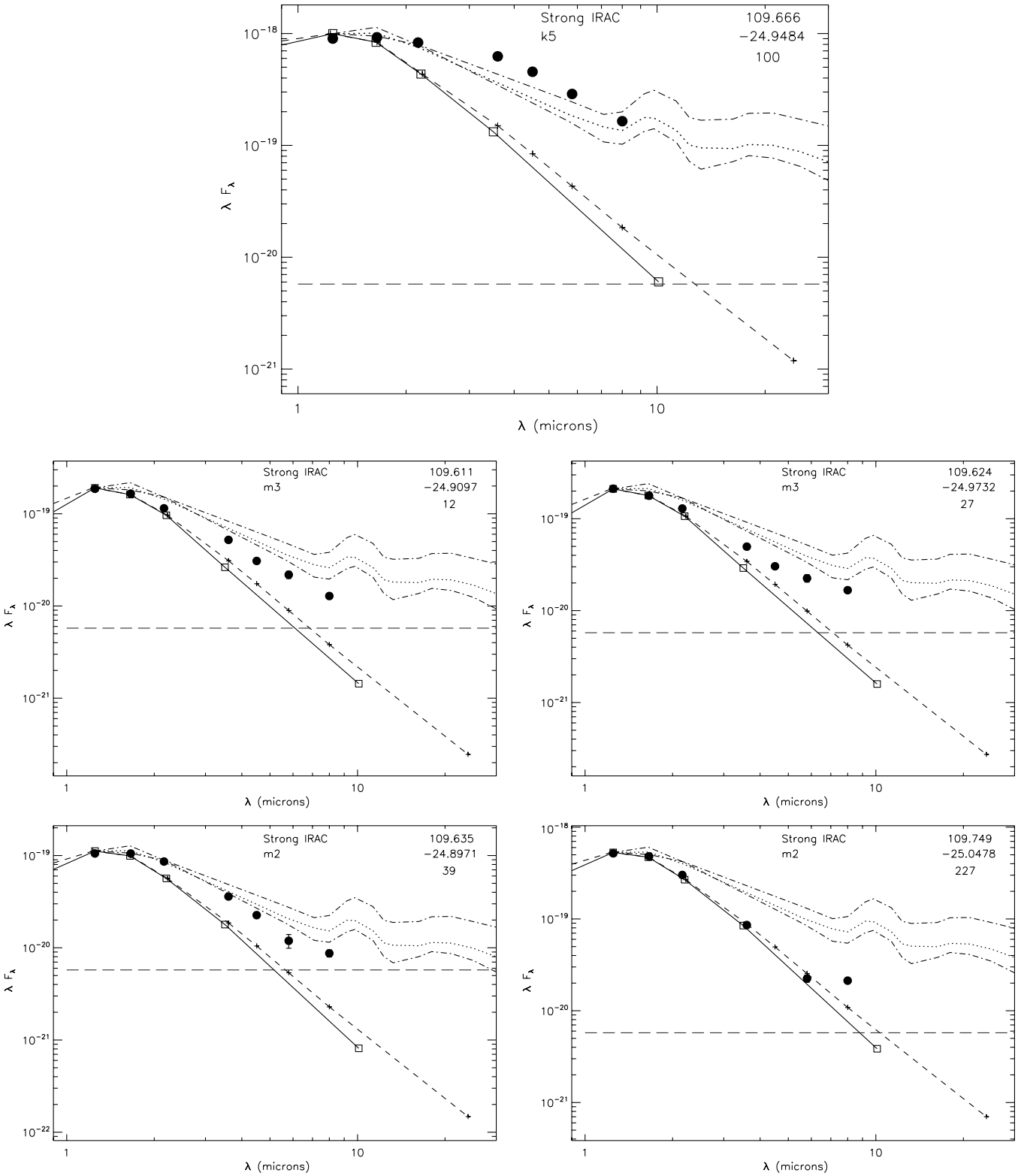


**Figure 11.** SEDs for primordial/evolved primordial disk candidates from the Dahm & Hillenbrand (2007) sample lacking MIPS detections. Symbols are the same as before.

### *4.2.3. Summary of SED Analysis*

Analyzing the SEDs of late-type, MIPS-detected NGC 2362 stars reveals disks with a wide range of evolutionary states. Primordial disks in NGC 2362 are very rare. Only 19% of the MIPS-detected confirmed/candidate cluster stars from Dahm & Hillenbrand (2007) have SEDs consistent with primordial disks. Combining the Dahm & Hillenbrand (2007) sample with the Irwin et al. (2008) sample of 14 MIPS-detected stars indicates that the true fraction of primordial disks in NGC 2362 is even lower, ∼17% (6/35).

Most disks surrounding late-type cluster stars are in an advanced evolutionary state. In the Dahm & Hillenbrand (2007) sample, ∼57% (12/21) of late-type, MIPS-detected sources have SEDs consistent with disks with a reduced mass at all disk radii (homologously depleted disks). If candidates from Irwin et al. (2008) are included, the fraction of these disks is ∼49% (17/35). Disks with inner holes/gaps (transition disks) also comprise a large fraction of MIPS-detected sources, representing ∼24% (5/21) of MIPS-detected Dahm & Hillenbrand sources and ∼34% (12/34) of all confirmed/candidate cluster members detected by MIPS. In total, 81% (83%) of the MIPS-detected late-type stars in the Dahm & Hillenbrand sample (Dahm & Hillenbrand+Irwin et al. samples combined) have disks in evolutionary states between primordial disks and debris disks. Any other disk-bearing stars lacking MIPS detections have 24 $\mu$m emission lying below the detection limit. Compared to the stars with MIPS detections, disks around these stars have even weaker emission suggestive of substantial evolution. Therefore, disks around most late-type stars in NGC 2362 are leaving the primordial disk phase.

Our results stand in contrast to those from Dahm & Hillenbrand (2007) who find that primordial disks comprise ∼34% of the total disk population. Our photometry identifies a comparable number of confirmed members with $\alpha \geqslant -1.8$ (16) and between −1.8 and −2.56 (30), so poorer photometry is unlikely to explain this discrepancy. However, many sources (e.g., ID 3) listed in Table 5 and identified as "primordial" disks by Dahm & Hillenbrand clearly have SEDs that do not look anything such as canonical primordial disks found in Taurus and other young star-forming regions. In part, some of these discrepancies result from the adopted definition of a primordial disk. In this paper, we define a primordial disk to be a disk with an SED close to the median Taurus SED and a disk mass $\gtrsim 10^{-3}$ $M_{\odot}$. Modeling shows that only five of the 16 stars with $\alpha \geqslant -1.8$ have SEDs and disk masses typical of primordial disks. Using only a single parameter (the IRAC slope) then results in a larger number of primordial disks than identified from full SED modeling.

## 5. IMPLIED CONSTRAINTS ON THE EVOLUTION OF CIRCUMSTELLAR DISKS AND PLANET FORMATION

The disappearance of primordial disks and the emergence of debris disks sets an empirical limit for the formation timescale of gas giant planets. The disappearance of IR excesses in disks implies the disappearance of the building blocks—solid material—for the cores of gas giant planets. Similarly, the lack of gas accretion implies a lack of circumstellar gas in inner disk regions, which corresponds to a lack of material to build the gaseous envelopes of gas giant planets. Therefore, in this section we use results from analysis presented in Section 4 to constrain the evolutionary states of disks and to investigate the formation timescale of gas giant planets as a function of stellar mass (Section 5.1). We divide the sample into high/intermediate-mass stars ($M_{\star} \gtrsim 1.4$ $M_{\odot}$) and solar/subsolar-mass stars ($\lesssim 1.4$ $M_{\odot}$).

From the population of NGC 2362 stars surrounded exclusively by debris disks, we compare their 24 $\mu$m debris luminosity with that for $\gtrsim$5 Myr old stars to investigate the evolution of debris emission and the connections this evolution has with the growth of icy planets (Section 5.2). In Section 5.3, we compare the more evolved primordial disk population to disks in other 1–10 Myr old clusters to examine the morphology of and timescale for the primordial-to-debris disk transition.

The results presented in this section are based on analyzing the *MIPS-detected* population of NGC 2362 confirmed/candidate members and other cluster stars with clear evidence for disks listed in Table 5. Most faint confirmed/candidate cluster stars are not detected by MIPS because of its bright 5$\sigma$ limit ([24] ∼ 10.5). Therefore, completeness at 24 $\mu$m may affect our results. However, we show that any disk-bearing sources not detected by MIPS either harbor debris disks or homologously depleted disks with low masses. MIPS is sensitive enough to detect levels of 24 $\mu$m emission typical of primordial disks surrounding faint cluster stars and emission typical of all but low-luminosity debris disks around brighter cluster stars. Thus, our ability to determine when primordial disks disappear is not undermined by sample incompleteness. Because different dust masses are implied for detections as opposed to nondetections, the detection limit may serve as a discriminator between disk types.

Because not all of the MIPS-detected members and candidate members have published spectral types, this section uses the $J$–$K_s$ color as a tracer of spectral type and thus, assuming a 4–5 Myr age, stellar mass. While the lack of published spectral types for some sources adds uncertainty to our analysis, known properties of NGC 2362 stars show that this uncertainty is not significant given the coarse division into stars with masses greater than or lesser than 1.4 $M_{\odot}$. NGC 2362 has a small dispersion in age (Mayne & Naylor 2008), which yields a reliable conversion from spectral type to stellar mass. The cluster also has a very low reddening ($E(B-V) \sim 0.1$), which translates into $E(J$–$K_s) \sim$0.05–0.06. For early-type, high/intermediate-mass stars (BAFG) to be misidentified as low-mass stars based on their observed $J$–$K_s$ colors, they must have a reddening ∼3–5 times the typical reddening of the cluster. There is little evidence for such a large spread in reddening. Cluster stars with known spectral types have $J$–$K_s$ colors consistent with using $J$–$K_s = 0.6$ as the division between high/intermediate-mass stars and low-mass stars.

### 5.1. Constraints on the Formation Timescale for Gas Giant Planets

Assuming an age of ∼4–5 Myr, NGC 2362 stars with masses >1.4 $M_{\odot}$ have G or earlier spectral types and $J$–$K_s < 0.6$ (Baraffe et al. 1998). Cluster stars with masses $\geqslant$2 $M_{\odot}$ have spectral types earlier than mid F and $J$–$K_s \lesssim$0.3 (Kenyon & Hartmann 1995; Siess et al. 2000). From Figure 6, the $K_s$–[24] upper limits for stars with $M_{\star}$ ∼1.4–2 $M_{\odot}$ are ∼2.5; the upper limits for more massive, 2 $M_{\odot}$ stars are ∼1–1.5. In comparison the predicted $K_s$–[24] excesses for primordial disks and transition disks discussed in Section 4 are ∼4–5.5 mag over this spectral type range. Thus, any primordial disks or transition disks around cluster stars with masses >1.4 $M_{\odot}$ are easily detectable. Stars with "homologously depleted" disks listed in Table 5 have $K_s$–[24] > 3 and are also easily detectable.

Analysis from Section 4 shows that there are no primordial disks, transition disks, or homologously depleted disks surrounding NGC 2362 stars plausibly in this mass range. MIPS-detected stars with $M_{\star} \geqslant 2$ $M_{\odot}$ have photospheric emission or $\lesssim$2 mag excesses (e.g., Figures 6 and 7). MIPS-detected stars with masses likely between 1.4 $M_{\odot}$ and 2 $M_{\odot}$ include only one star, ID 144, with nonphotospheric emission. high/intermediate-mass cluster stars with optical spectra do not show any evidence for $H_{\alpha}$ emission indicative of gas accretion.

Based on SED modeling and dust removal timescales (Section 4), all disks surrounding high/intermediate-mass cluster stars are debris disks. Furthermore, even though *Spitzer* observations only trace thermal emission from small circumstellar dust grains not gas, the observable signatures of disks in evolutionary states with gas (primordial, transition, homologously depleted) are clearly lacking from any high/intermediate-mass star studied here. NGC 2362 then lacks any disks around high/intermediate-mass stars which have yet to reach the debris disk phase. Recent combined *Spitzer* and ground-based surveys of young clusters indicate that circumstellar gas should disperse on similar or faster timescales than dust (Lada et al. 2006). If this is the case, our results suggest that gas giant planet formation likely occurs prior to 4–5 Myr for $>1.4\ M_{\odot}$ stars.

MIPS-detected late-type stars in NGC 2362 have inferred masses between $\sim 0.3\ M_{\odot}$ and $1.4\ M_{\odot}$ (e.g., Baraffe et al. 1998; Siess et al. 2000; Dahm & Hillenbrand 2007). Most late-type stars detected by MIPS have SEDs consistent with more evolved primordial disks or debris disks. About 1/3 of MIPS-detected disks in the Dahm & Hillenbrand (2007) sample are transition disks. Nearly half of all MIPS-detected stars are surrounded by disks that are depleted in mass at a range of disk radii (homologously depleted). There is no clear connection between disks with this morphology and active planet formation. Only four stars have SEDs consistent with primordial disks. Given the MIPS detection limit for this sample, we can rule out the presence of any $\gtrsim$4.5 mag excesses typical of primordial disks and transition disks.

Disks surrounding late-type stars in NGC 2362 that are not detected by MIPS must have $K_s$–[24] $\leqslant$ 4–4.5. These disks are likely either debris disks or homologously depleted disks with levels of emission slightly below the MIPS detection limit. The disk population of solar and subsolar-mass stars is dominated by the large number of MIPS upper limits, making statistically robust conclusions about the bulk disk population difficult. However, combined with the low frequency of accretion in NGC 2362 (Dahm 2005a; Dahm & Hillenbrand 2007), these results demonstrate that most disks surrounding late-type stars have significantly evolved and that most lack evidence for circumstellar gas needed to form gas giant planets.

While some primordial disks remain around $\lesssim 1.4\ M_{\odot}$ stars, the disk population for these stars is dominated by disks which have clearly undergone a significant amount of evolution (transition disks, homologously depleted disks). The morphologies of transition disks and homologously depleted disks are consistent with disks actively leaving the primordial disk phase for the debris disk phase. If these disks are actively making the primordial-to-debris disk transition, then gas giant planet formation also likely ceases by $\approx$5 Myr for many, perhaps most, solar/subsolar-mass stars.

### 5.2. Debris Disk Evolution around High/Intermediate-Mass Stars

Combining NGC 2362 data for high/intermediate-mass stars with data from other clusters probes the time evolution of debris emission from planet formation. Specifically, we examine the time evolution of 24 $\mu$m excess emission (see also Rieke et al. 2005; Su et al. 2006; Hernandez et al. 2006; Currie et al. 2008a; Wyatt 2008), focusing on 5–40 Myr old early-type stars. We include all confirmed/candidate high/intermediate-mass members in NGC 2362 with MIPS detections. In addition to our data, we include stars from clusters with debris disks: Orion OB1a and b (10 and 5 Myr; Hernandez et al. 2006), $\eta$ Cha (8 Myr; Gautier et al. 2007), the $\beta$ Pic Moving Group (12 Myr; Rebull et al. 2008), $h$ and $\chi$ Persei ($\sim$13 Myr; Currie et al. 2008a), Sco-Cen, and NGC 2547 (38 Myr; Rieke et al. 2005). For the Sco-Cen, we include data for Upper Scorpius (5 Myr), Upper Centaurus Lupus (16 Myr), and Lower Centaurus Crux (17 Myr) from Chen et al. (2005). We limit our literature sample to BAF stars.

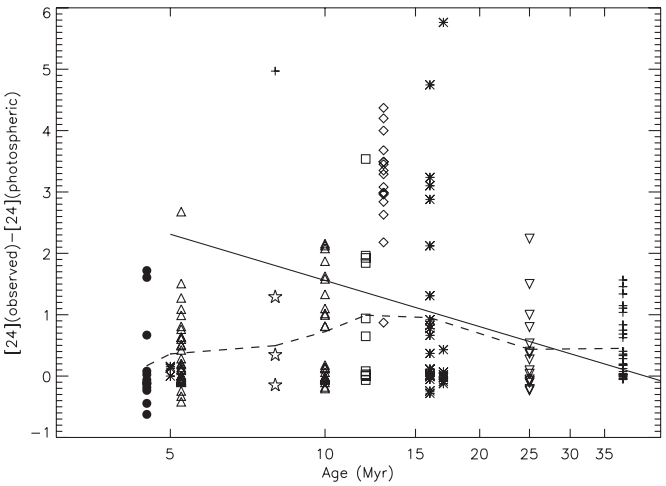


**Figure 12.** Amplitude of 24 $\mu$m excess around BAF stars vs. time for 4–40 Myr old clusters. Besides NGC 2362 (filled dots), we include Orion Ob1a and b (10 and 5 Myr; triangles), $\eta$ Cha (8 Myr; stars), the $\beta$ Pic Moving Group (12 Myr; squares), $h$ and $\chi$ Persei (13 Myr; diamonds), Sco-Cen (5, 16, and 17 Myr; asterisks), NGC 2232 (25 Myr; inverted triangles), and NGC 2547 (38 Myr; small crosses). HR 4796A, from Low et al. (2005) is also shown as a cross at $t \sim 8$ Myr and $[24]–[24]_{\rm phot} \sim 5$. The data are consistent with a rise in debris emission from 5 Myr to 10 Myr, a peak from $\sim$10 Myr to 20 Myr as shown previously by Currie et al. (2008a). For stars older than $\approx$40 Myr, the distribution of 24 $\mu$m luminosity defines an envelope which is consistent with a $t^{-1}$ decline (Rieke et al. 2005). The dashed line shows the mean excess. Predictions for the decline in emission from a steady-state collisional evolution model (triple-dot-dashed) follow a $t^{-1}$ decline.

Figure 12 shows the individual amplitudes of 24 $\mu$m excesses as a function of time. In support of Currie et al. (2008a), there is a rise in the level of debris emission from $\sim$5 Myr to 10 Myr and a peak at $\sim$10–20 Myr (see also Currie et al. 2008b). Rieke et al. (2005) show that the emission at later ages ($\gtrsim$30–50 Myr) is consistent with a $1/t$ decline (dot-dashed line). The mean level of excess (dashed line) for $\lesssim$20 Myr old clusters clearly deviates from a $t^{-1}$ decline.

MIPS data for NGC 2362 stars supports the trend of debris disk evolution from 5 Myr to 10 Myr first identified by Currie et al. (2008a). Three clusters/associations in Figure 12 have ages of $\sim$5 Myr: Orion OB1b, Upper Scorpius, and NGC 2362. All three clusters/associations have levels of excess that are weaker than those for $\sim$10–15 Myr old clusters, Orion Ob1a, the $\beta$ Pic Moving Group, $h$ and $\chi$ Persei, and Upper Centaurus Lupus. Debris disks in 5 Myr old clusters also have lower 24 $\mu$m luminosities than those in 25–40 Myr old clusters NGC 2232 and NGC 2547 (Currie et al. 2008b; Rieke et al. 2005). The conclusion that debris disks surrounding early-type, high-mass stars exhibit a "rise" and "fall" trend (Currie et al. 2008a) instead of a monotonic decline in emission (e.g., Rieke et al. 2005) is now very robust.

The observed behavior of debris disk evolution agrees well with predictions from sophisticated debris disk models. Kenyon & Bromley (2008) investigate the evolution of debris emission from icy planet formation in disks surrounding $\gtrsim 1\ M_{\odot}$ stars. For

$\sim$2 $M_{\odot}$ stars with a disk mass of $\sim$2–3 times a scaled Minimum Mass Solar Nebula, 24 $\mu$m debris emission rises rapidly from $\sim$5 Myr to $\sim$8 Myr after the start of the simulation which is sustained for $\approx$20 Myr. *Spitzer* observations indicate a $\approx$3 Myr lifetime for primordial disks around these stars (Hernandez et al. 2007a; Currie & Kenyon 2009). The Kenyon & Bromley models would then predict an observed peak in 24 $\mu$m debris emission by $\sim$8–11 Myr that lasts through $\approx$30 Myr. These expectations agree with the trend shown in Figure 12.

Within the context of the Kenyon & Bromley (2008) models, the trend in 24 $\mu$m debris emission is directly linked to the growth of icy planets. The Kenyon & Bromley simulations start with a swarm of $\approx$0.1–10 km-sized planetesimals. These bodies rapidly grow to $\approx$100–1000 km sizes within several Myr in the *runaway growth* phase (Wetherill & Stewart 1993). Once icy bodies grow to $\gtrsim$1000 km sizes, they stir the leftover planetesimals to much higher velocities. These higher velocities reduce the gravitational focusing factor of the growing planets, and the planets enter the much slower *oligarchic* growth phase. The higher velocities also cause more energetic collisions between planetesimals, causing more fragmentation and increasing the dust production rate. Because small dust is needed to make debris disks visible in the mid-IR, Kenyon & Bromley (2008) identify the onset of oligarchic growth with the peak in debris disk luminosity. Therefore, the Kenyon & Bromley models associate the systematically weaker excesses for $\approx$5 Myr old stars with an early stage in planet formation where icy bodies are $\lesssim$1000 km in size and actively growing. Similarly, the models associate the stronger excesses surrounding 10–30 Myr old stars with later stages in planet formation where some icy bodies are $\gtrsim$1000 km in size and are growing at slower rates.

### *5.3. Constraints on the Primordial-to-Debris Disk Transition for Solar/Subsolar-Mass Stars*

The large number of stars with disks in an intermediate stage between primordial disks and debris disks allows us to investigate the primordial-to-debris disk transition in detail. Our results challenge conventional ideas about two aspects of the primordial-to-debris disk transition: the morphology of disks in such an intermediate stage and the timescale for transition.

In agreement with previous *Spitzer* work, particularly Lada et al. (2006), our results indicate the existence of at least two evolutionary paths from primordial disks to debris disks. Many MIPS-detected cluster members have transition disk morphologies with SEDs showing weak, optically thin emission through $\approx$5–8 $\mu$m but strong, optically thick emission by $\approx$24 $\mu$m. However, many more stars are surrounded by homologously depleted disks whose mass is likely lost at all disk radii simultaneously. While 24 $\mu$m emission for transition disks is stronger than for homologously depleted disks, homologously depleted disks typically have stronger $\lesssim$8 $\mu$m emission. It is unlikely that either of these morphologies is the evolutionary precursor of the other. Thus, strictly speaking, there is more than one type of "transition disk". Both morphologies can be thought of as "evolved primordial disks" since the disk characteristics suggest they are more likely to be composed of first generation dust, not second generation dust (i.e., debris disks).

Our results also place new constraints on the timescale for the transition from primordial disks to debris disks. According to studies of disks in young, $\lesssim$3 Myr old clusters, most notably Taurus–Auriga, the paucity of transition disks relative to primordial disks implies that the transition timescale is $\lesssim 10^5$ yr (Skrutskie et al. 1990; Hartigan et al. 1990; Simon & Prato 1995; Wolk & Walter 1996). Our work and other recent work (e.g., Haisch et al. 2001; Hernandez et al. 2007a) indicates that the lifetime of primordial disks surrounding many young stars is $\sim$3–5 Myr. In this picture, the lifetime of the primordial disk phase is $\gtrsim$30–50 times the lifetime of the transition disk phase. However, if disks spend a factor of 30–50 times longer in the primordial disk phase, then primordial disks should always be far more numerous than transition disks. If, on the other hand, the transition disk and primordial disk lifetimes are comparable, then transition disks should be equal to or greater in number than primordial disks by $\approx$5 Myr.

Based on these data, the traditional arguments favoring a $\lesssim 10^5$ yr transition timescale are incorrect. For the MIPS-detected Dahm & Hillenbrand (2007) sample, transition disks are equal in number to primordial disks. When the Irwin et al. (2008) sample of candidate members is included, transition disks are about twice as numerous as primordial disks. Many disks are also homologously depleted and represent a separate evolutionary path from primordial disks to debris disks. The combined population of MIPS-detected homologously depleted disks and transition disks in the Dahm & Hillenbrand sample are more numerous than primordial disks by a factor of $\sim$4. When the Irwin et al. (2008) data are included, they dominate over the primordial disk population by 6 to 1. Even if the homologously depleted disks with the strongest mid-IR emission (IDs 36, 85, 204, 214, and 251) were all reclassified as primordial disks, primordial disks would still comprise less than half of the total disk population for late-type stars. Because many homologously depleted disks may have 24 $\mu$m fluxes lying just below the MIPS detection limit, the population of disks in between primordial and debris disks may be even more numerous.

Our results strongly favor a longer, $\sim$1 Myr timescale for the primordial-to-debris disk transition for disks with ages $\sim$5 Myr. Besides this work, there is evidence in favor of such a trend from other recent *Spitzer* surveys. *Spitzer* observations of some $\lesssim$5 Myr old clusters reveal a substantial population of transition disks and homologously depleted disks consistent with $\sim$1 Myr timescale for the primordial-to-debris disk transition. MIPS-detected disks showing evidence for substantial evolution in 2–3 Myr old IC 348, labeled *anemic* disks in Lada et al. (2006), comprise $\approx$40%–45% of all MIPS-detected disks (Currie & Kenyon 2009), a fraction much higher than that for Taurus–Auriga. SED analysis of these sources shows that about two-thirds are homologously depleted disks and one-third are transition disks (Lada et al. 2006; Currie & Kenyon 2009). *Spitzer* photometry and IRS spectroscopy of low-mass stars in the $\approx$1 Myr old Coronet Cluster also reveal a population of transition disks and homologously depleted disks whose high frequency is in conflict with a $\lesssim 10^5$ yr transition timescale (Sicilia-Aguilar et al. 2008).

These evolved primordial disks also dominate over primordial disks in at least two samples of $\gtrsim$5 Myr old stars. Most sources with optically thick mid-IR emission from the FEPS sample (ages $\sim$3–30 Myr) have SEDs indicating that their disks' inner regions are cleared of dust to distances probed by $\sim$3.6–8 $\mu$m (Hillenbrand et al. 2008). In four of the six stars shown in Hillenbrand et al. (2008), the SEDs rise from 8–13 $\mu$m to $\sim$24 $\mu$m as in transition disks. The remaining two stars have SEDs showing excess emission weaker than that of typical primordial disks and indicative of homologously depleted disks studied here. The 2MASS/IRAC survey of $h$ and $\chi$ Persei (13–14 Myr) fail to detect any stars with clear $K$-band excess

emission indicative of primordial disks but find that ∼4%–8% have 8 $\mu$m excess emission (Currie et al. 2007c). While most of these stars likely harbor warm debris disks, several sources analyzed further in Currie et al. (2007a) and one analyzed in Currie et al. (2008a), have accretion signatures and/or mid-IR colors suggestive of evolved primordial disks.

## 6. SUMMARY AND DISCUSSION

In this paper, we analyze *Spitzer* data for the ∼5 Myr old cluster NGC 2362 to explore the primordial-to-debris disk transition and the formation timescale for gas giant planets. From the list of confirmed/candidate cluster members, we analyze mid-IR colors, compare source SEDs to disk models representing a range of evolutionary states, and compare SEDs to signatures of gas accretion to constrain the evolutionary state of disks. Then we compare the properties of disks surrounding high-to-low-mass stars to constrain the timescale for gas giant planet formation. From the sample of early-type, high/intermediate-mass stars with debris disks, we investigate the evolution of debris emission from planet formation. Finally, we study the morphology of disks evolving from primordial disks to debris disks and place limits on the timescale for this transition.

### 6.1. Overview of Results

Our study yields the following major results.

1. For all stellar masses, NGC 2362 contains very few stars surrounded by primordial disks with strong near-to mid-IR emission characteristic of 1 Myr old stars in Taurus. The disk population is dominated by evolved primordial disks, whose SEDs are indicative either of so-called transition disks (inner holes/gaps) or homologously depleted disks.
2. NGC 2362 lacks any stars with masses $\gtrsim$1.4 $M_{\odot}$ that have primordial disks which comprise the building blocks of giant planets. These stars also lack evidence for having transition or homologously depleted disks. Because most disks surrounding 1 Myr old stars show evidence for protoplanetary disks, gas giant planets surrounding $\gtrsim$1.4 $M_{\odot}$ stars likely form in ≈1–5 Myr.
3. Most disks surrounding solar/subsolar-mass stars are either transition disks or homologously depleted disks and thus are likely in the process of dispersing. Some disks may be debris disks, indicating that any gas giant planet formation has ceased. Thus, gas giant planets may form by ∼4–5 Myr for stars with a wide range of masses.
4. Both canonical transition disks and homologously depleted disks represent an evolutionary pathway from primordial disks to debris disks (see also Lada et al. 2006). Furthermore, there are a large number of these evolved primordial disks compared to primordial disks. This work and previous work suggests that primordial disks have a typical lifetime of ∼3–5 Myr. Thus, the timescale for the primordial-to-debris disk transition must be $\gg$0.1 Myr and may be roughly comparable to the primordial disk lifetime (e.g., ≈1 Myr). A ≈1 Myr timescale for this evolution is inconsistent with published models predicting a rapid transition.

### 6.2. On the Primordial-to-Debris Disk Transition

Despite sample incompleteness in MIPS for the faintest cluster stars, the presence of debris disks around the high/intermediate-mass stars and presence of at least many primordial disks and evolved primordial disks around lower-mass stars in NGC 2362 is consistent with the stellar-mass-dependent evolution of primordial disks found in other recent *Spitzer* studies. Lada et al. (2006) showed that disks in 2–3 Myr old IC 348 exhibit a spectral type/stellar-mass-dependent frequency of warm dust from disks with the frequency peaking for early M stars. Hernandez et al. (2007a) also find a stellar-mass-dependent frequency of warm dust in 3 Myr old $\sigma$ Orionis.

Moreover, our work suggesting that debris disks may emerge faster around high/intermediate-mass stars supports the study of 5 Myr old Upper Scorpius from Carpenter et al. (2006). Carpenter et al. (2006) find that high/intermediate-mass stars in Upper Scorpius not only have a lower frequency of disk emission compared to low-mass stars but also have a lower 16 $\mu$m disk luminosity. While Carpenter et al. (2006) do not model the disk emission from high/intermediate-mass stars to demonstrate that these stars are surrounded by debris disks, they do note that the weak 16 $\mu$m emission and lack of accretion signatures for these stars are consistent with debris disk characteristics. This work and that of Carpenter et al. combined then provide strong evidence that debris disks dominate the disk population of high/intermediate-mass stars by ∼5 Myr. Analysis of the disk population around high-mass stars in IC 348 indicate that debris disks may emerge even sooner (Currie & Kenyon 2009).

A ≈1 Myr timescale for the primordial-to-debris disk transition undermines the viability of UV photoevaporation as the primary physical process by which most primordial disks disappear as presented in published models from Alexander et al. (2006) and Clarke et al. (2001). In standard photoevaporation models (e.g., Alexander et al. 2006), once stellar accretion rates drop below the photoevaporative mass-loss rate active disk dispersal can commence. Once this condition is met, primordial disks are completely dispersed within ∼0.01–0.1 Myr. Alexander et al. (2006) showed that disks dispersing by UV photoevaporation follow clear evolutionary tracks in their mid-IR colors: stars with colors consistent with bare photospheres and colors consistent with primordial disks should *always* be more frequent than those with intermediate colors. In contrast, our results find that disks in an intermediate stage dominate over primordial disks. The inside-out dispersal of disks in photoevaporation models is also not consistent with the morphology of homologously depleted disks, which comprise the plurality of MIPS-detected disks in NGC 2362.

The only way in which the NGC 2362 data is consistent with a very rapid transition timescale expected from standard photoevaporation models is if the spread in primordial disk lifetimes is very narrow ($\ll$1 Myr) and with a mean value of ≈4 Myr (R. Alexander 2008, private communication). However, if this were the case for all clusters, plots of the disk frequency versus time for clusters (e.g., Haisch et al. 2001; Hernandez et al. 2007a) would look more like a step function than a steady decline. Analysis of *Spitzer* data for other clusters both younger (Cha I, IC 348, $\sigma$ Ori) and older (TW Hya Association, 25 Ori) suggest a larger spread in lifetimes (Luhman et al. 2008; Lada et al. 2006; Hernandez et al. 2007a; Low et al. 2005; Hernandez et al. 2007b). For each cluster, especially those older than ∼2–3 Myr, there exists a wide diversity of disk properties. Some stars around 2–3 Myr old stars have very weakly emitting, highly evolved disks or lack any evidence for a disk (Lada et al. 2006). Conversely, ∼5–10 Myr old clusters have some stars with

primordial disks, homologously depleted disks, or canonical transition disks (e.g., Low et al. 2005; Hernandez et al. 2007b). For photoevaporation models to be consistent with observed disk properties, initial parameters (e.g., extreme-ultraviolet flux, $\alpha$ viscosity parameter) must be fine-tuned to yield a far longer disk transition timescale. It is unclear whether these models can modified in such a way.

Because our results do not find evidence for a rapid transition timescale, the supposedly rapid timescale for all disks as inferred from Taurus data must have alternate explanations. Stars in Taurus show an apparently rapid transition timescale because of two main factors: (1) their youth and (2) binarity. First, previous *Spitzer* studies indicate that the typical primordial disk lifetime is at least $\sim$3 Myr (Lada et al. 2006; Hernandez et al. 2007a), which is older than the median age of Taurus ($\sim$1–2 Myr). Therefore, most disks in Taurus (1–2 Myr) are too young to have begun leaving the primordial disk phase. The frequency of transition or homologously depleted disks compared to primordial disks for Taurus should then be low as observed. While it is possible that some stars (e.g., those in Taurus) make the primordial-to-debris transition in $\sim 10^5$ yr, our results indicate that a more typical transition timescale is far longer.

Second, binarity affects primordial disk evolution. Ireland & Kraus (2008) show that CoKu Tau/4, long regarded a prototypical transition disk, is actually a short-period binary system. Its lack of warm dust emission is due to tidal interactions with the faint binary companion and not from physical processes typically associated with transition disks (e.g., planet formation, photoevaporation). Recent high-contrast imaging of Taurus stars without disks indicate that a large number of them also have short-period binaries (A. Kraus et al. 2009, in preparation). Because binary companions are responsible for clearing these disks, the true number of stars lacking a disk because of standard disk dispersal processes (grain growth, accretion, planet formation, photoevaporation) is likely *far* lower than previously thought. Therefore, the small fraction of transitional disks in Taurus and other young star-forming regions does not necessarily mean that the typical transition timescale due to disk processes is rapid.

### 6.3. Implications for the Formation of Gas Giant Planets, and Future Work

Combined with results from previous work, the most straightforward interpretation of our results is that gas giant planets have to form sometime between 1 Myr and 4–5 Myr around most stars or else they will not form at all. We acknowledge that the strength of this conclusion is limited by using indirect tracers for the presence of gas-rich primordial disks for many stars. It is also possible that the absolute age calibration of NGC 2362 is uncertain by several Myr. Nevertheless, a short, 1–5 Myr formation timescale for gas giant planets is in strong agreement with timescales inferred from properties of our solar system's planets and satellites. For instance, a 1–5 Myr timescale is consistent with the results of Castillo-Rogez et al. (2007) who argue that Saturn formed as early as 2.5 Myr after the formation of calcium–aluminum-rich inclusions (CAIs), whose formation may have been contemporaneous with the birth of the Sun and the solar nebula.

A short formation gas giant formation timescale presents a challenge for core accretion models of gas giant planet formation. Many detailed models of planet formation (e.g., Alibert et al. 2005) assume that circumstellar disks with initial masses comparable to the Minimum Mass Solar Nebula are depleted by only factors of $\sim$2–5 by $\sim$5 Myr. Our analysis suggests that primordial disks may not last this long. Other models (e.g., Dodson-Robinson et al. 2008) claiming to form gas giants within $\sim$3–5 Myr rely on simple treatments of core growth that neglect important effects such as the evolution of the planetesimal velocity distribution and collisional fragmentation of planetesimals. To date, only the model of Kenyon & Bromley (2009) has successfully modeled the formation of gas giant planet cores in $\lesssim$5 Myr while properly incorporating these first-order effects. The relative timescales for core growth and the dispersal of primordial disks may explain trends in exoplanet properties (Currie 2009).

In spite of the failure of most core accretion models to form gas giant planets in less than 5 Myr while accounting for important effects, radial velocity surveys indicate that gas giants are common (Cumming et al. 2008). Moreover, gas giants may be most frequent around high/intermediate-mass stars (Johnson et al. 2007). Our results imply that the formation timescales for gas giants around these stars are probably much shorter compared to those for lower-mass stars. If gas giants form by core accretion then their formation, especially around high/intermediate-mass stars, must be very rapid and efficient.

Recent and upcoming *Spitzer* surveys provide an opportunity to explore the primordial-to-debris disk transition and planet formation timescales further. Unpublished *Spitzer* IRS data as well as Cycle 5 IRAC and MIPS observations of massive clusters (e.g., Upper Scorpius and $h$ and $\chi$ Persei) strengthen constraints on the primordial-to-debris disk transition at $\sim$5 Myr and probe this transition at later, $\sim$10–15 Myr, ages. Combined with this study, these surveys should result in strong constraints on the evolution of disks from the primordial disk-dominated epoch ($\lesssim$5 Myr) to the debris disk-dominated epoch ($\gtrsim$5–15 Myr) and yield the most definitive statements on the timescale for planet formation from the *Spitzer Space Telescope* mission.

We thank Richard Alexander for useful comments about UV photoevaporation and Adam Kraus for very informative discussions on the role of binarity in disk evolution. We also thank Carol Grady for pointing out constraints on the formation of Saturn from the planetary science community. Support for this work was provided by NASA through the *Spitzer Space Telescope* Fellowship Program (TPR).

*Facility: Spitzer Space Telescope*

## APPENDIX A

## A COMPARISON BETWEEN OUR IRAC PHOTOMETRY AND THAT FROM DAHM & HILLENBRAND (2007)

Our primary motivation for redoing IRAC photometry of NGC 2362 is to identify candidate cluster stars with mid-IR excesses at $\leqslant$10 $\mu$m from the Irwin et al. (2008) catalog and to construct full SEDs from $V$ band through 24 $\mu$m to constrain the origin of the emission in all cluster stars. To test the accuracy of our IRAC photometry, we compare it with photometry from Dahm & Hillenbrand (2007). Because Dahm & Hillenbrand (2007) only publish photometry for cluster members, our analysis in this section is limited to the 337 Dahm & Hillenbrand (2007) (candidate) members.

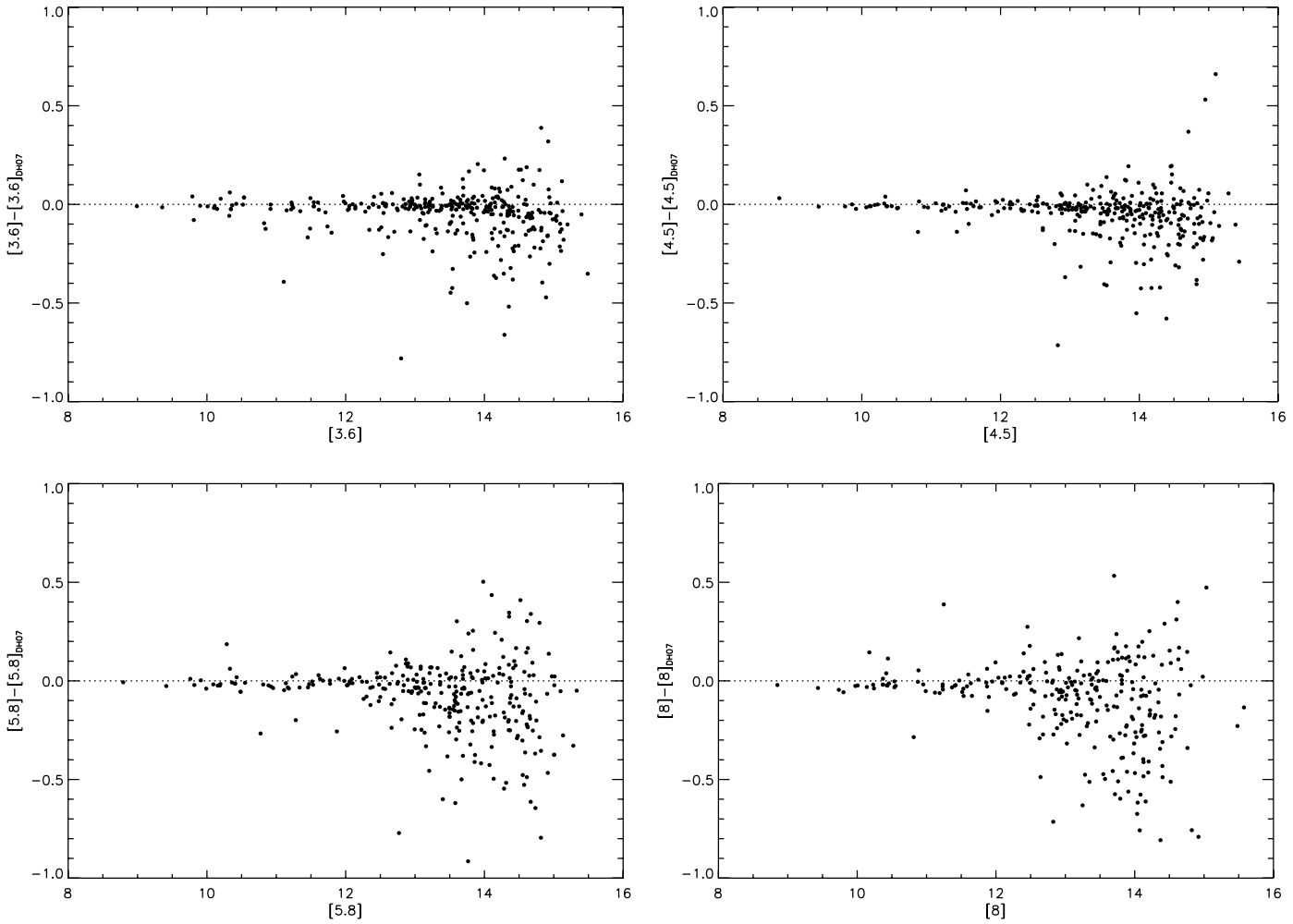


**Figure 13.** Difference between our IRAC photometry and that from Dahm & Hillenbrand (2007) as a function of our IRAC magnitude. The Dahm & Hillenbrand (2007) photometry exhibits a deflection toward fainter magnitudes as a function of survey depth ($\delta$(IRAC) < 0).

Figures 13 and 14 contrast our photometry with that of Dahm & Hillenbrand (2007). In Figure 13, we show the difference in magnitude for each IRAC channel as a function of (our) magnitude. Photometry from both groups appears to have little/no zero-point offset. However, the Dahm & Hillenbrand (2007) photometry exhibits a deflection toward fainter magnitudes for $m$(IRAC) $\gtrsim 13$ in all filters relative to our photometry. This effect is especially pronounced in the [5.8] and [8], which clearly show a non-Gaussian scatter.

Figure 14 shows that the mid-IR colors also have systematic differences. The top panels compare the distributions of $J$–$K_s$ versus $K_s$–[8] colors. We have far fewer sources with unphysical $K_s$–[8] colors (less than −0.2): the blue limit of the $K_s$–[8] distribution tracks the photospheric locus (solid line) very well. The $K_s$–[8] colors from Dahm & Hillenbrand (2007) deflect blueward of the photospheric locus by up to 0.5–1. Our photometry includes only two stars with $K_s$–[8] $\sim -0.2$ compared to 17 in Dahm & Hillenbrand (2007). The [5.8] versus [3.6]–[5.8] distribution for our sources (middle panels) also contains fewer stars with very blue ([3.6]–[5.8] < −0.5) colors and exhibits a smaller dispersion in color, especially for stars fainter than $m$[5.8] = 13.

In the bottom panels of Figure 14, we quantify the differences in photometry at 4.5 $\mu$m and 8 $\mu$m by fitting a line (dash-dotted) to the 8 $\mu$m to 4.5 $\mu$m flux ratio (log(F[8]/F[4.5])) as a function of $J$–$K_s$ color (see also Carpenter et al. 2006; Currie et al. 2008b) for sources with 5$\sigma$ detections in both filters. As in Carpenter et al. (2006) and Currie et al. (2008b), the best-fit line is determined by a linear least-squares fit with 4$\sigma$ clipping to remove outlying sources, including stars with IR excess. The dispersion and rms residuals are then recalculated. The Dahm & Hillenbrand (2007) photometry has a 3$\sigma$ dispersion in log(F[8]/F[4.5]) of ∼0.23 and residuals in the linear fit of ∼5.5%. Five stars with larger photometric uncertainties have negative flux ratios that lie outside the dispersion (dashed lines). Our photometry has a dispersion of 0.16% and 4.3% fit residuals with one outlying star. Furthermore, four stars in the Dahm & Hillenbrand (2007) photometry have extremely negative flux ratios, lying 5–6$\sigma$ fainter than the photospheric locus. If the distribution in flux ratios followed a normal distribution, we would expect, at most, one such source. Our photometry contains just one 3$\sigma$ outlier with a negative flux ratio.

The differences in photometry are primarily due to the smaller aperture radius employed here (2 pixels vs. 3 pixels in Dahm &

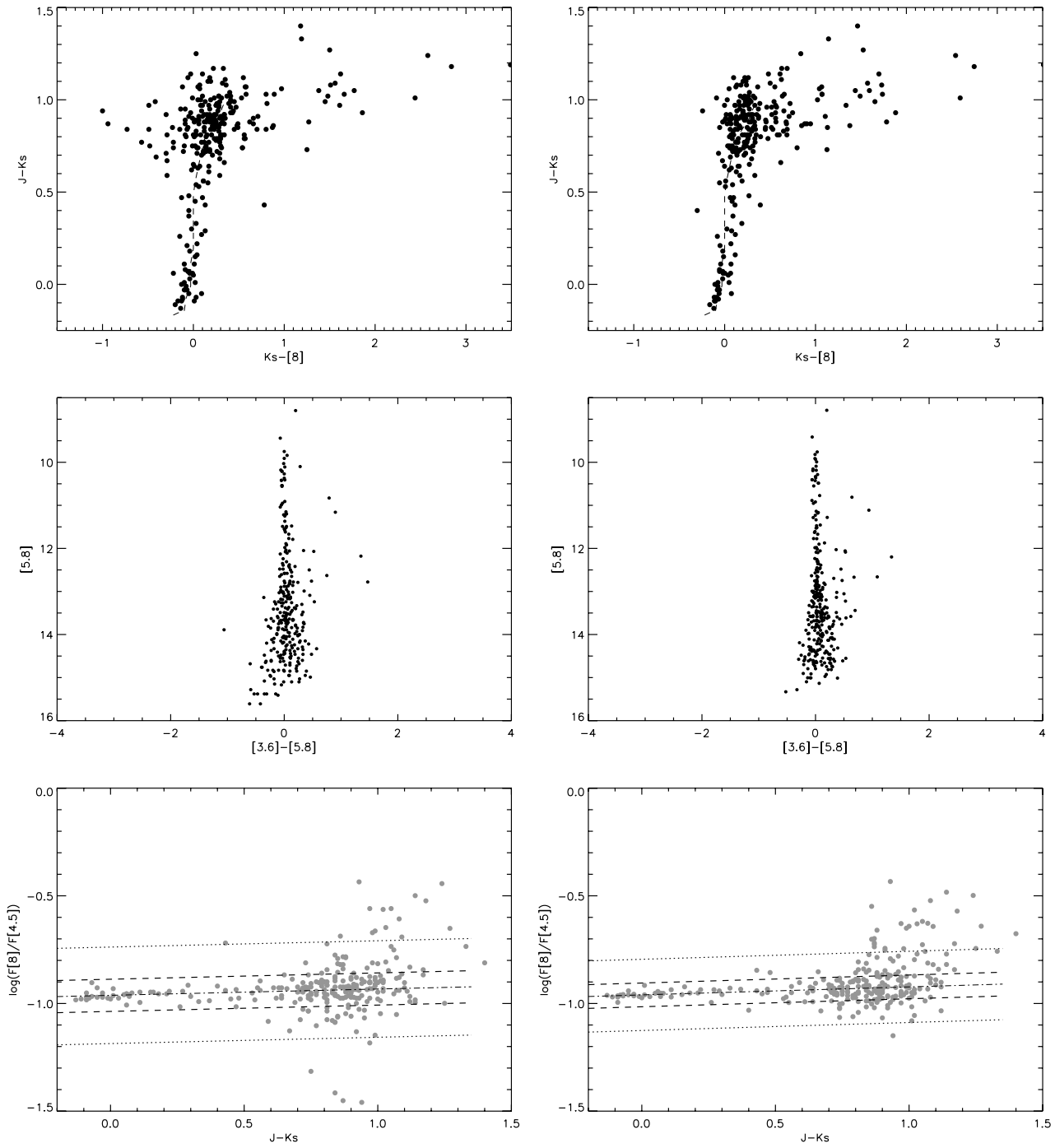


**Figure 14.** IRAC colors from Dahm & Hillenbrand (2007, left columns) and this work (right columns). Top: the $J$–$K_s$ vs. $K_s$–[8] color–color diagram for sources in common between Dahm & Hillenbrand (2007) and this work. Middle: [5.8] vs. [3.6]–[5.8] color–magnitude diagrams. Bottom: the 8 $\mu$m to 4.5 $\mu$m flux-ratio diagram for the same samples. The best-fit line (dash-dotted line) and 3$\sigma$ dispersion above and below the best-fit line (dashed lines) are overplotted. The Dahm & Hillenbrand (2007) photometry yields many stars with unphysically blue 2MASS/IRAC colors ($K_s$–[8] $\leqslant -0.2$; [3.6]–[5.8] $\leqslant -0.5$) and unphysically small flux ratios ($\leqslant -1.15$). The photometry from this work lacks many blue colors and exhibits less far scatter, especially at fainter magnitudes in the 8 $\mu$m channel.

Hillenbrand 2007). The sky background may be overestimated from the larger sky annulus needed for a 3 pixel aperture in densely populated regions, which results in artificially faint sources whose colors deflect blueward. Differences in image processing methods may also explain differences in photometry. Differences in the aperture radius and image processing methods have led to significant discrepancies in photometry for other *Spitzer* cluster data. In these cases, more accurate photometry was also obtained using a smaller aperture radius (e.g., Cha I; Luhman et al. 2008).

## APPENDIX B

## ATLAS OF SEDS OF MIPS-DETECTED (CANDIDATE) CLUSTER MEMBERS

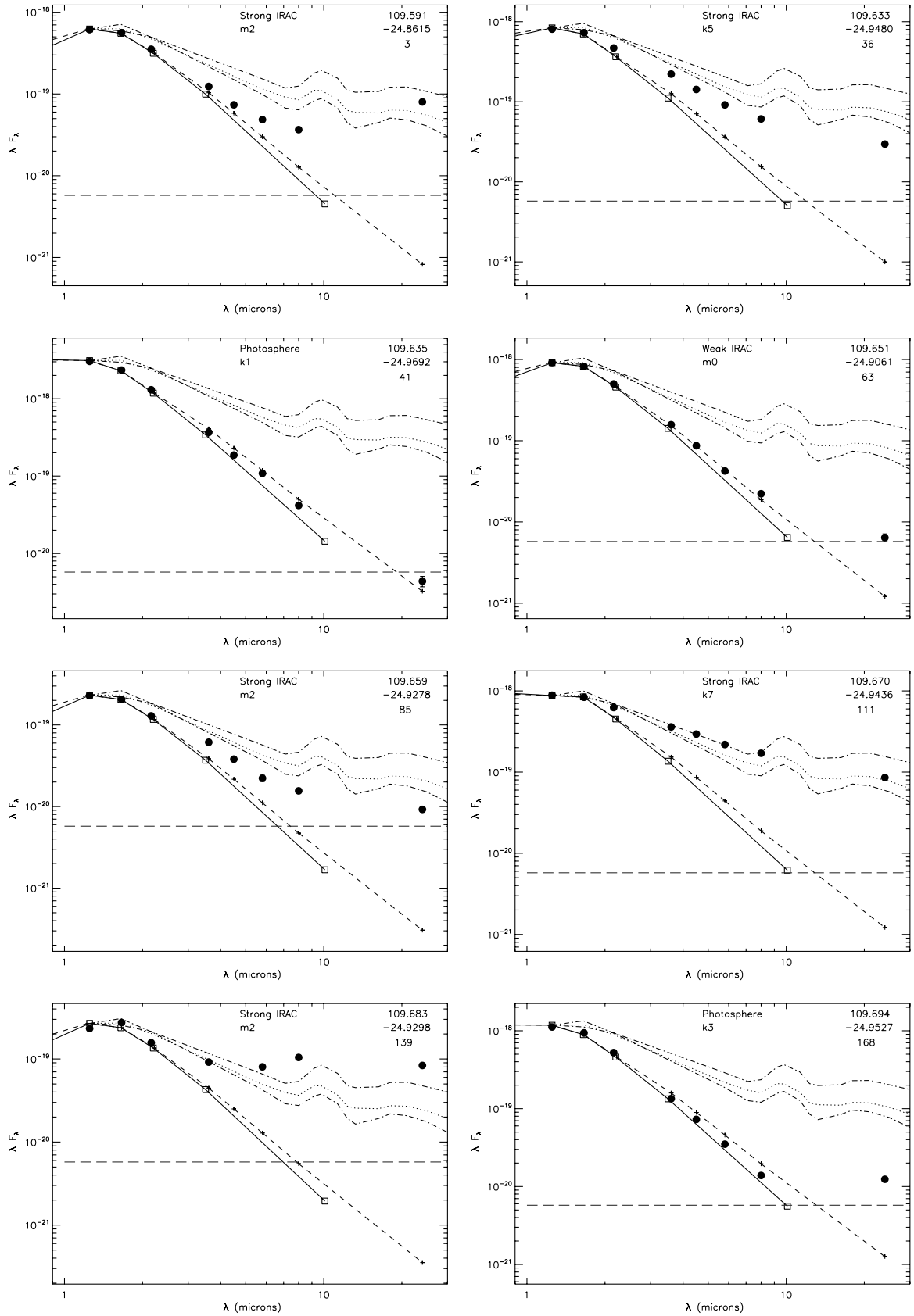


**Figure 15.** Atlas of SEDs of late-type NGC 2362 members with MIPS 24 $\mu$m excesses. Overplotted are the median Taurus SED (dotted line) with upper and lower quartiles (dot-dashed line). A terrestrial zone debris disk model is shown as a dashed line with mid-IR flux slightly greater than the photosphere (solid line, connected by open squares). The MIPS 5$\sigma$ detection limit is shown as a horizontal gray dashed line.

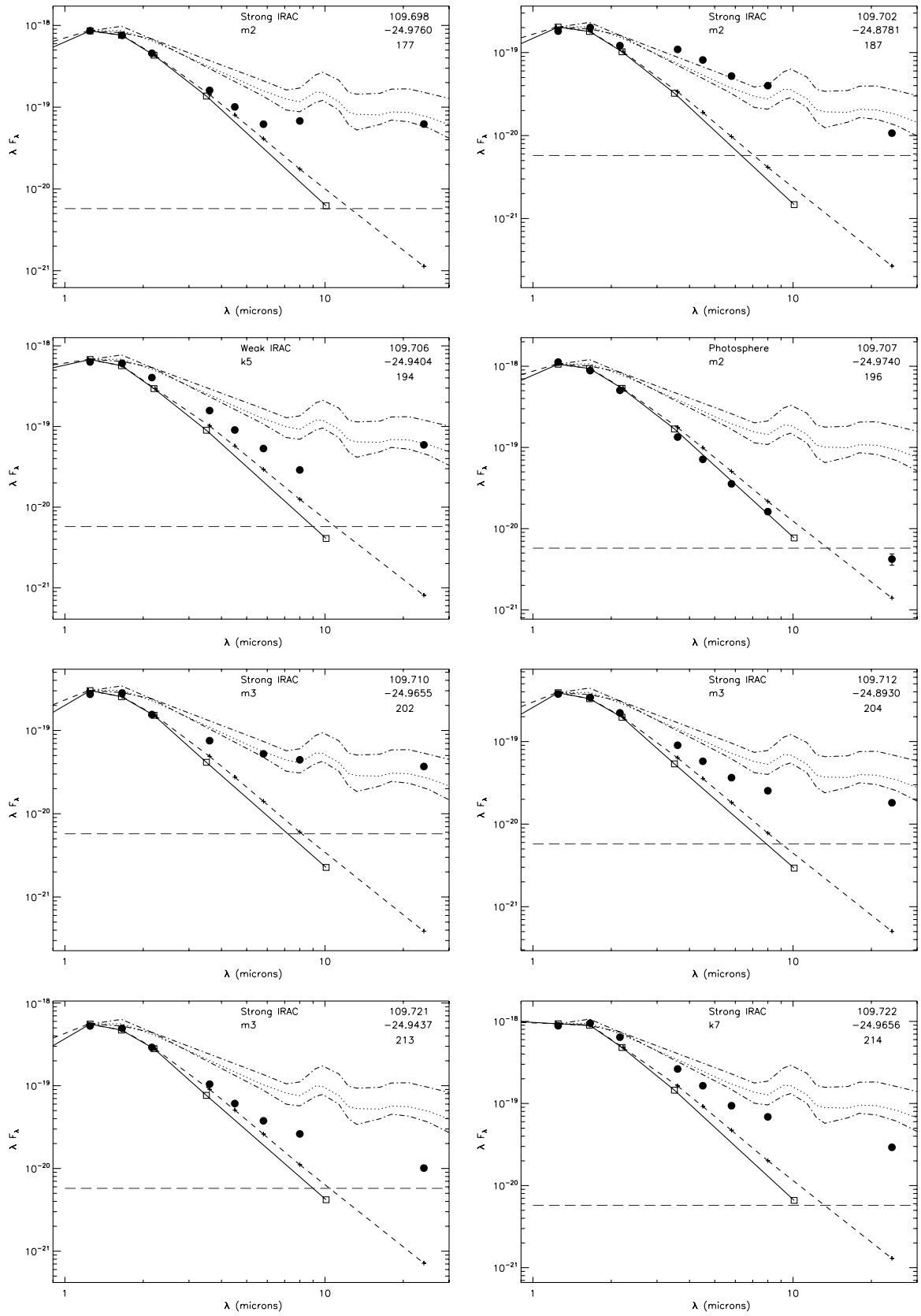


**Figure 16.** Same as Figure 15.

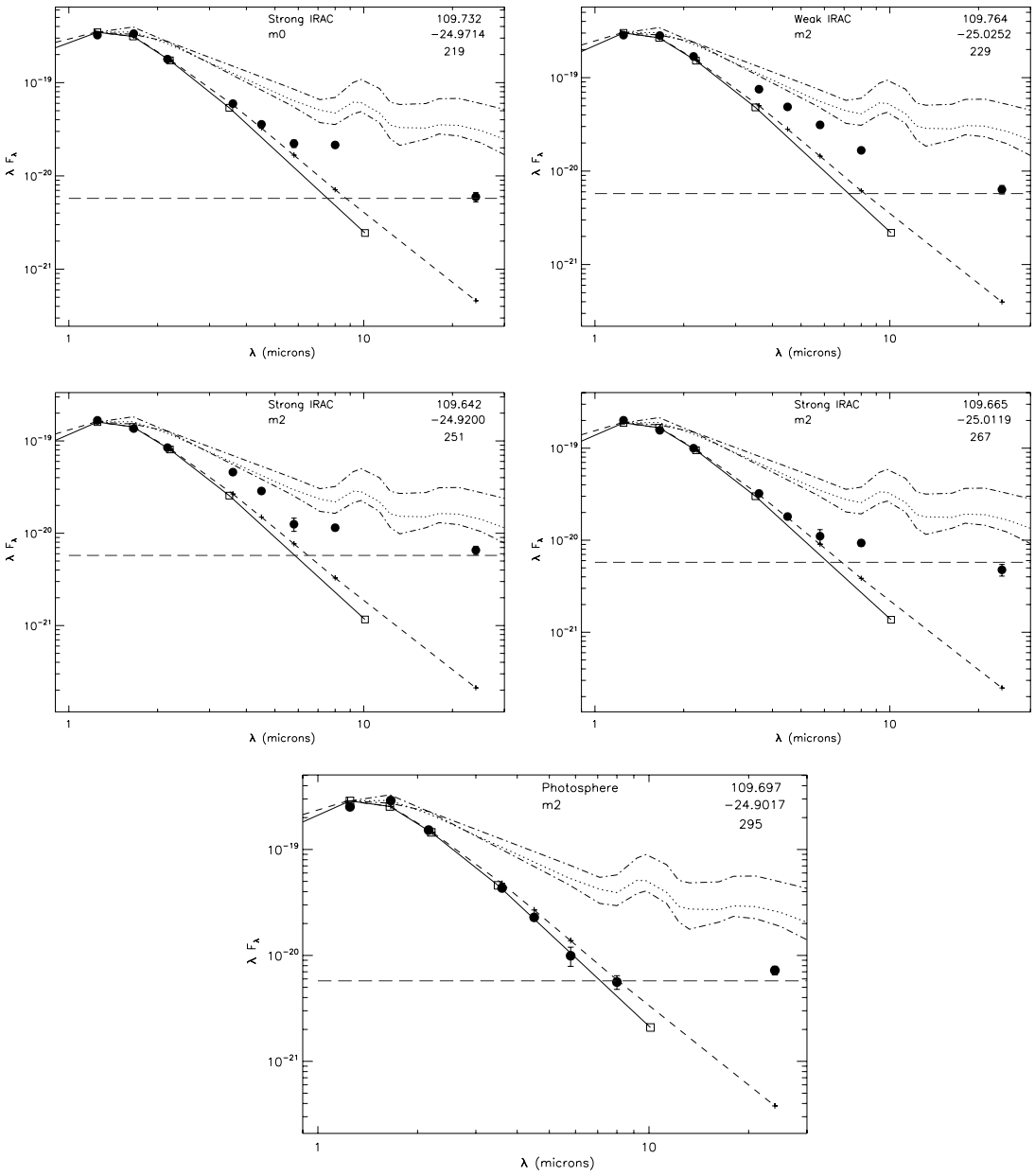


**Figure 17.** Same as Figures 15 and 16.

## REFERENCES


Aigrain, S., et al. 2007, MNRAS, 375, 29
Alexander, R., Clarke, C. J., & Pringle, J. E. 2006, MNRAS, 369, 229
Alibert, Y., Mordasini, C., Benz, W., & Winisdoerffer, C. 2005, A&A, 434, 343
Andrews, S. M., & Williams, J. P. 2005, ApJ, 631, 1134
Augereau, J., Lagrange, A. M., Mouillet, D., Papaloizou, J. C. B., & Grorod, P. A. 1999, A&A, 348, 557
Backman, D., & Paresce, F. 1993, in Protostars and Planets III, ed. E. H. Levy, J. I. Lunine (Tucson, AZ: Univ. Arizona Press), 1253
Balona, L. A., & Laney, C. D. 1996, MNRAS, 281, 1341
Baraffe, I., et al. 1998, A&A, 337, 403
Bertin, E., & Arnouts, S. 1996, A&AS, 117, 393
Burns, J., Lamy, P. L., & Soter, S. 1979, Icarus, 40, 1
Calvet, N., et al. 2005, ApJ, 630, L185
Carpenter, J., Mamajek, E., Hillenbrand, L., & Meyer, M. 2006, ApJ, 651, L49
Castillo-Rogez, J. C., Matson, D., Sotin, C., Johnson, T. V., Lunine, J., & Thomas, P. 2007, Icarus, 190, 179
Chen, C., Jura, M., Gordon, K. D., & Blaylock, M. 2005, ApJ, 623, 493
Chen, C., & Kamp, I. 2004, ApJ, 602, 985
Chen, C., et al. 2006, ApJS, 166, 351
Clarke, C. J., Gendrin, A., & Sotomayor, M. 2001, MNRAS, 328, 485
Cumming, A., et al. 2008, PASP, 120, 531
Currie, T. 2005, ApJ, 629, 549
Currie, T. 2008, PhD thesis, Univ. California-Los Angeles
Currie, T. 2009, ApJ, 694, L171
Currie, T., & Kenyon, S. J. 2009, submitted (arXiv:0801.1116)
Currie, T., Kenyon, S., Balog, Z., Bragg, A., & Tokarz, S. 2007a, ApJ, 669, L33
Currie, T., Kenyon, S., Balog, Z., Rieke, G., Bragg, A., & Bromley, B. 2008a, ApJ, 672, 558
Currie, T., Kenyon, S., Rieke, G., Balog, Z., & Bromley, B. 2007b, ApJ, 663, L105
Currie, T., Plavchan, P., & Kenyon, S. J. 2008b, ApJ, 688, 597
Currie, T., et al. 2007c, ApJ, 659, 599
Currie, T., et al. 2009, AJ, 137, 3210
Dahm, S. 2005a, AJ, 130, 1805
Dahm, S. 2005b, PhD thesis, Univ. Hawaii-Manoa
Dahm, S., & Hillenbrand, L. 2007, AJ, 133, 2072
Dodson-Robinson, S., et al. 2008, ApJ, 688, L99
Fazio, G., et al. 2004, ApJS, 154, 10
Forbrich, J., et al. 2008, ApJ, 687, 1107
France, K., Roberge, A., Lupu, R., Redfield, S., & Feldman, P. 2007, ApJ, 668, 1174

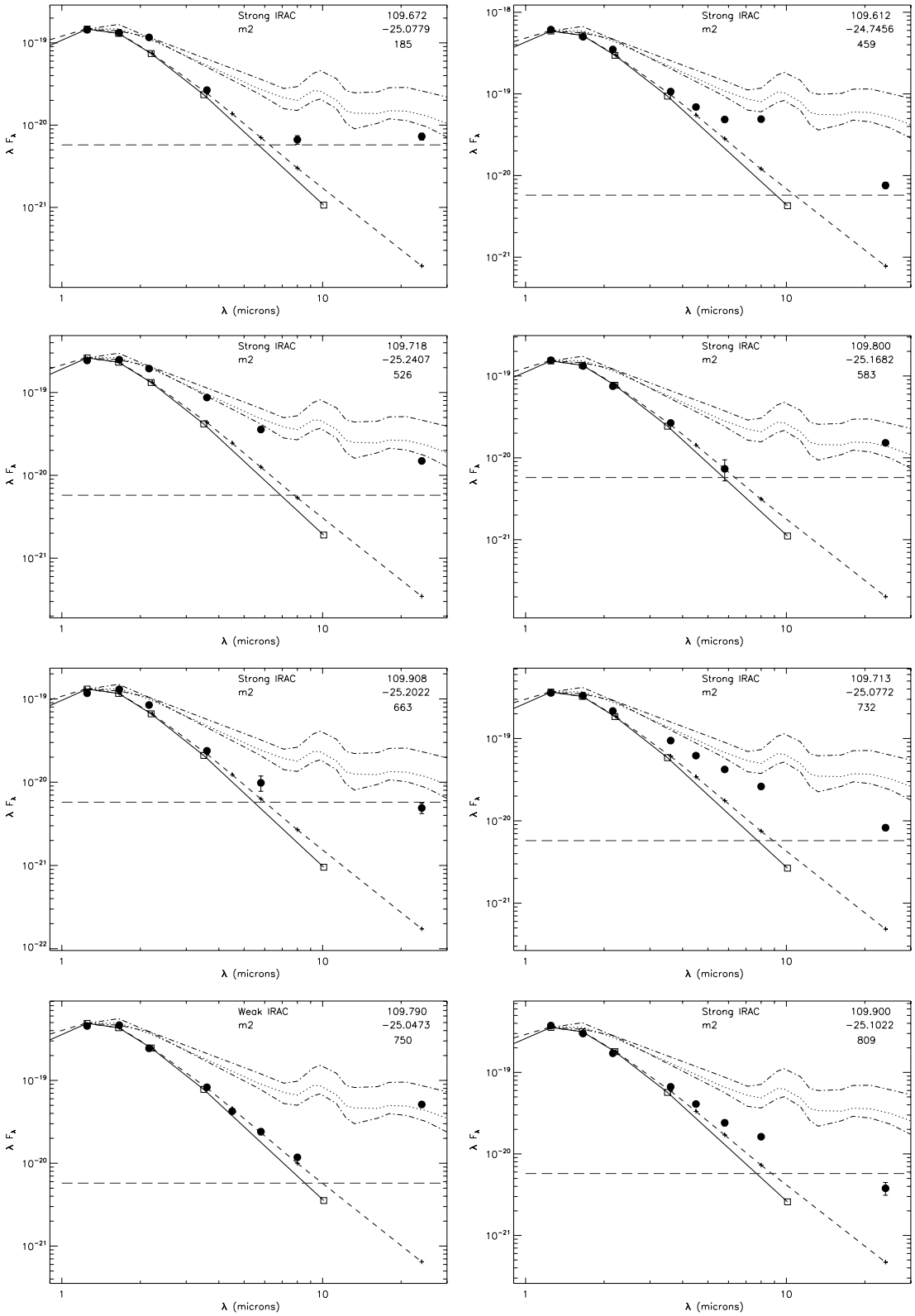


**Figure 18.** SEDs for MIPS-detected candidates from the Irwin et al. (2008). Symbols are the same as in the preceding figures.

Furlan, E., et al. 2006, ApJS, 165, 568
Gautier, T., et al. 2007, ApJ, 667, 527
Haisch, K., Lada, C., & Lada, E. 2001, ApJ, 553, L153
Hartigan, P., Hartmann, L., Kenyon, S. J., Strom, S., & Skrutskie, M. 1990, ApJ, 354, L25
Hernandez, J., Briceno, C., Calvet, N., Hartmann, L., Muzerolle, J., & Quintero, A. 2006, ApJ, 652, 472
Hernandez, J., et al. 2007a, ApJ, 662, 1067
Hernandez, J., et al. 2007b, ApJ, 671, 1784
Hillenbrand, L., et al. 2008, ApJ, 677, 630
Ireland, M. J., & Kraus, A. L. 2008, ApJ, 678, L591
Irwin, J., et al. 2008, MNRAS, 384, 675
Johnson, J. A., et al. 2007, ApJ, 670, 833
Kenyon, S., & Bromley, B. 2004, ApJ, 602, L133

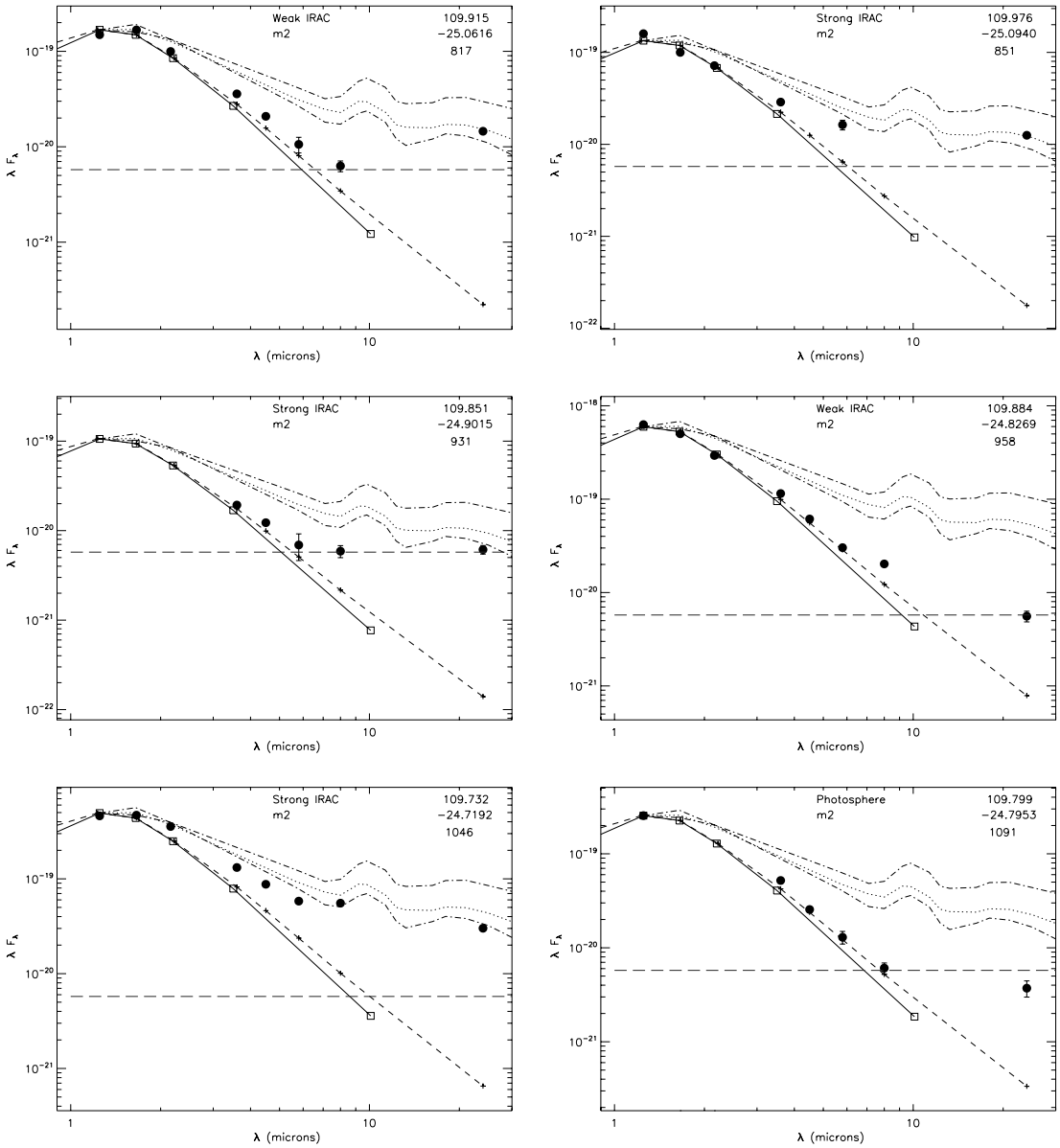


**Figure 19.** Same as Figure 18.


Kenyon, S., & Bromley, B. 2008, ApJS, 179, 451
Kenyon, S., & Bromley, B. 2009, ApJ, 690, L140
Kenyon, S., & Hartmann, L. 1995, ApJS, 101, 117
Kurucz, R. L. 1993, SYNTHE Spectrum Synthesis Programs and Line Data, Kurucz CD-ROM 18 (Cambridge, MA: Smithsonian Astrophysical Observatory), 18
Lada, C. J., & Adams, F. C. 1992, ApJ, 393, 278
Lada, C. J., et al. 2006, AJ, 131, 1574
Lejeune, Th., Cuisinier, F., & Buser, R. 1997, A&AS, 125, 229
Low, F., Smith, P., Werner, M., Chen, C., & Jura, M. 2005, ApJ, 631, 1170
Luhman, K., et al. 2008, ApJ, 675, 1375
Lyra, W., et al. 2006, A&A, 453, 101
Makovoz, D., & Khan, I. 2005, PASP, 347, 81
Makovoz, D., & Marleau, F. 2005, PASP, 117, 1113
Mathis, J. 1990, ARA&A, 28, 37
Mayne, N. J., & Naylor, T. 2008, MNRAS, 386, 261
Moitinho, A., Alves, J., Huelamo, N., & Lada, C. J. 2001, ApJ, 563, L73
Plavchan, P., et al. 2005, ApJ, 631, 1161
Plavchan, P., et al. 2009, ApJ, in press (arXiv:0904.0819)
Pollack, J., et al. 1996, Icarus, 124, 62
Preibisch, T., & Feigelson, E. 2005, ApJS, 160, 390
Quijada, M., et al. 2004, in Proc. SPIE 5487 Optical, Infrared, and Millimeter Space Telescopes, ed. J. C. Mather (Bellingham, WA: SPIE), 244
Rafikov, R. 2004, AJ, 128, 1348
Rebull, L., et al. 2008, ApJ, 681, 1484
Rice, W. K., & Armitage, P. 2003, ApJ, 598, L55
Rieke, G., et al. 2004, ApJS, 154, 25
Rieke, G., et al. 2005, ApJ, 620, 1010
Rieke, G., et al. 2008, AJ, 135, 2245
Roberge, A., & Weinberger, A. 2008, ApJ, 676, 509
Robin, A. C., et al. 2003, A&A, 409, 523
Robitaille, T., et al. 2006, ApJS, 167, 256
Robitaille, T., et al. 2007, ApJS, 169, 328
Sicilia-Aguilar, A., et al. 2008, ApJ, 687, 1145
Siess, L., Dufour, E., & Forestini, M. 2000, A&A, 358, 593
Simon, T., & Prato, L. 1995, ApJ, 450, 824
Skrutskie, M., Dutkevitch, D., Strom, S., Edwards, S., Strom, K., & Shure, M. 1990, AJ, 99, 1187
Strubbe, L., & Chiang, E. 2006, ApJ, 648, 652
Su, K., et al. 2006, ApJ, 653, 675
Takeuchi, T., & Artymowicz, P. 2001, ApJ, 557, 990
Wetherill, G., & Stewart, G. 1993, Icarus, 106, 190
White, R. J., & Basri, G. 2003, ApJ, 582, 1109
Wolk, S. J., & Walter, F. 1996, AJ, 111, 2066
Wood, K., Lada, C. J., Bjorkman, J. E., Kenyon, S. J., Whitney, B., & Wolff, M. 2002, ApJ, 567, 1183
Wyatt, M. 2008, ARA&A, 46, 339
Zuckerman, B., Forveille, T., & Kastner, J. H. 1995, Nature, 373, 494